

**REPUBLIC OF TURKEY  
YILDIZ TECHNICAL UNIVERSITY  
GRADUATE SCHOOL OF NATURAL AND APPLIED SCIENCES**

**CHARACTERIZATION OF TiO<sub>2</sub>/Cu<sub>2</sub>O THIN FILM PHOTOVOLTAIC CELLS**

**TÜLİN YILMAZ**

**MSc. THESIS  
DEPARTMENT OF CHEMICAL ENGINEERING  
PROGRAM OF CHEMICAL ENGINEERING**

**ADVISER  
PROF. DR. HANİFİ SARAÇ**

**İSTANBUL, 2014**

**REPUBLIC OF TURKEY**  
**YILDIZ TECHNICAL UNIVERSITY**  
**GRADUATE SCHOOL OF NATURAL AND APPLIED SCIENCES**

**CHARACTERIZATION OF TiO<sub>2</sub>/Cu<sub>2</sub>O THIN FILM PHOTOVOLTAIC CELLS**

A thesis submitted by Tülin YILMAZ in partial fulfillment of the requirements for the degree of **MASTER OF SCIENCE** is approved by the committee on 24.09.2014 in Department of Chemical Engineering, Chemical Engineering Program.

**Thesis Adviser**

Prof.Dr. Hanifi SARAÇ

Yıldız Technical University

**Approved By the Examining Committee**

Prof.Dr.Hanifi SARAÇ

\_\_\_\_\_

Doç.Dr.Fatme Jale GÜLEN

\_\_\_\_\_

Doç.Dr.Kaan YETİLMEZSOY

\_\_\_\_\_

This study was supported by the ERASMUS 2013 – 2014 education and training program at University of Twente Inorganic Materials Science Group.

## ACKNOWLEDGEMENTS

---

This master thesis is the result of my study at Chemical Engineering Department at Yıldız Technical University. It has been prepared during Erasmus education and training program at University of Twente Inorganic Materials Science Group (IMS). At this time period, research and experiments have been studied in a European project which is called “Novel Composite Oxides for Next Generation All-Oxide Photovoltaics” with collaborations from different countries; Spain, Israel, Germany, and Portugal. During this study I had very valuable support from many people. I would like to express my grateful acknowledgement to all of them.

Firstly, I would like to thank to Prof.Dr.Hanifi Saraç for his supervision through this study and his encouragement for my abroad experience.Furthermore, I would like to thank you Dr.Ir.Mark Huijben from University of Twente in the Netherlands, for his kind and supportive guidance before I came to Netherlands and also for giving me opportunity of being a part of IMS group.I’m sincerely grateful to my daily supervisor Tom Wijnands for sharing with me all his knowledge and experiences, understanding my lack of knowledge, caring my all weird questions and trying to answer them every time patiently.

I am also thankful to everybody in IMS for their friendliness and helpfulness. It was very efficient and matchless experience for me as working in this research project Therefore, being here was gained to me a different perspective as learning new things day by day.

Finally, I would like to express adoringly my deep gratitude to my parents Tülay-İlhan Yılmaz, my sister Pelin Yılmaz and all of my friends, for their moral support and encouragement during through this long way.

June, 2014

Tülin YILMAZ

## TABLE OF CONTENTS

	Page
LIST OF SYMBOLS .....	vii
LIST OF ABBREVIATIONS .....	viii
LIST OF FIGURES.....	ix
LIST OF TABLES.....	xii
ABSTRACT.....	xiii
ÖZET .....	xv
CHAPTER 1	
INTRODUCTION.....	1
1.1 Literature Review .....	1
1.2 Objective of Thesis.....	3
1.3 Hypothesis .....	4
CHAPTER 2	
PHOTOVOLTAIC TECHNOLOGY .....	5
2.1 Photovoltaic Effect.....	6
2.1.1 Band Gap.....	6
2.1.2 Doping.....	8
2.1.3 Semiconductor materials.....	9
2.2 Photovoltaic Characterization .....	12
2.3 Spectral Nature of Sunlight.....	14
2.4 Classification of Solar Cells .....	15
2.4.1 Industrial solar cells .....	15
2.4.2 Pre-Industrial solar cells.....	19
CHAPTER 3	
FABRICATION OF THIN FILMS FOR PHOTOVOLTAIC APPLICATIONS .....	25
3.1 Chemical Deposition .....	25
3.1.1 Chemical solution deposition .....	25
3.1.2 Spin coating.....	26
3.1.3 Chemical vapor deposition .....	26
3.2 Physical Deposition .....	27

3.2.1 Sputter processing .....	27
3.2.2 Pulsed laser deposition .....	28
CHAPTER 4	
EXPERIMENTAL DETAILS .....	32
4.1 p-n Heterojunction Photovoltaic Cell Process Conditions.....	34
4.1.1 Sample preparation for deposition.....	35
4.1.2 TiO <sub>2</sub> deposition on FTO substrate.....	35
4.1.3 Sample cleaning after deposition .....	36
4.1.4 TiO <sub>2</sub> deposition on ITO substrate.....	38
4.1.5 Active layer deposition .....	38
4.1.6 Overall photovoltaic cell deposition .....	38
4.1.7 Bottom layer deposition (back contact) .....	39
4.2 Sample Inspection and Characterization .....	40
4.2.1 Illumination set-up.....	40
CHAPTER 5	
RESULTS AND DISCUSSION .....	46
5.1 TiO <sub>2</sub> Deposition Conditions.....	46
5.1.1 TiO <sub>2</sub> deposition on FTO substrate.....	46
5.1.2 TiO <sub>2</sub> deposition on ITO substrate.....	50
5.1.3 Active layer deposition .....	54
5.1.4 Overall photovoltaic cell deposition .....	58
CHAPTER 6 .....	62
CONCLUSIONS.....	62
REFERENCES.....	64
CURRICULUM VITAE.....	69

## LIST OF SYMBOLS

---

$E_g$	Band gap energy
$E_v$	Valance band energy
$E_c$	Conductance band energy
$E_\lambda$	Photon energy
VB	Valance band
CB	Conductance band
E	Internal electric field
$h\nu$	Incident photon energy
I	Net current
$I_0$	Saturation current density
$V_a$	Applied voltage
$I_{ph}$	Photogeneration current
$V_{oc}$	Open circuit voltage
$I_{sc}$	Short circuit current
$P_{max}$	Peak power
FF	Fill factor
$V_{mp}$	Voltage at maximum power point
$I_{mp}$	Current at maximum power point
$P_{in}$	Input power
$A_f$	Proportional constant
A	Absorption coefficient
d	Film thickness
$\lambda$	Wavelength
$\Omega$	Resistivity

## LIST OF ABBREVIATIONS

---

AM	Air mass
AZO	Aluminum doped zinc oxide
CdTe	Cadmium telluride
CIGS	Copper indium gallium selenide
CSD	Chemical solution deposition
CVD	Chemical vapor deposition
DSSC	Dye sensitized solar cell
FTO	Fluorine doped tin oxide
IEA	International Energy Agency
ITO	Tin doped Indiumoxide
IZO	Indium oxide doped zinc oxide
KrF	Krypton fluoride
MO	Metal oxide
PLD	Pulsed laser deposition
PV	Photovoltaic
PVD	Physical vapor deposition
SP08	Silicon solar cell
TCO	Transparent conductive oxide
ZO	Zinc oxide
$\alpha$ -Si	Amorphous silicon



## LIST OF FIGURES

		Page
Figure 1.1	Total energy sources (left) and evolution of world total primary energy supply (Mtoe) [1] .....	2
Figure 2.1	Evolution of global PV cumulative installed capacity 2000-2012 (GW) [3] .....	5
Figure 2.2	PV Opportunity mapping of sunbelt countries [3] .....	6
Figure 2.3	VB and CB in conductor, semiconductor and insulator [6] .....	7
Figure 2.4	Conduction and valence band positions for direct (left) and indirect (right) band gap .....	7
Figure 2.5	n-type silicon (top) and p-type silicon (bottom) by doping[11] .....	9
Figure 2.6	Diffusion and depletion region in p-n junction .....	10
Figure 2.7	p-n junction under reverse bias .....	11
Figure 2.8	p-n junction under forward bias.....	11
Figure 2.9	I-V characteristic of a p-n junction[14].....	12
Figure 2.10	I-V characteristic of a p-n junction in the dark and under illumination[14] .....	13
Figure 2.11	Standard spectral geometry[15].....	15
Figure 2.12	Monocrystalline silicon solar cell (left) and polycrystalline silicon solar cell (right) .....	17
Figure 2.13	CdTe thin film solar cell (left), record holder multi-junction solar cell (right) .....	19
Figure 2.14	Principle of dye sensitized photovoltaic cell (S:Sensitizer, S <sup>*</sup> :electronically excited sensitizer, S <sup>+</sup> : oxidized sensitizer)[27].....	20
Figure 2.15	(a) Schematic diagram of Cu <sub>2</sub> O/TiO <sub>2</sub> core shell p-n junction photovoltaic, (b) Energy band diagram of Cu <sub>2</sub> O/TiO <sub>2</sub> p-n junction, (c) I-V characteristics before and (d) after annealing in Ar at 200° C for 1 h[33] .....	21
Figure 2.16	(left) Energy level band diagram, (right) the current-voltage characteristics of the Cu <sub>2</sub> O/TiO <sub>2</sub> thin film (a) in the dark (b) under illumination [35] .....	22
Figure 2.17	Schematic cross-section of the completed structure[36] .....	23
Figure 2.18	Schematic drawing of the Au/Cu <sub>2</sub> O/ZnO nanowires/AZO/ITO/glass heterostructure solar cell [38].....	24
Figure 3.1	CVD mechanism [43] .....	26
Figure 3.2	Schematic representation of sputtering process .....	28
Figure 3.3	Etching illustration.....	28
Figure 3.4	Schematic diagram of PLD setup in University of Twente [48].....	29

Figure 3.5	Scalping the synthesis of nanaomaterials: from 5x5 mm <sup>2</sup> to 200 mm wafer size [48].....	30
Figure 4.1	Crystal forms of TiO <sub>2</sub> [53] .....	33
Figure 4.2	Crystal forms of copper oxide (gray:copper and red:oxygen atoms)[54] .	33
Figure 4.3	Pulsed laser deposition in University of Twente .....	36
Figure 4.4	Absorbance spectra of yellowish-glass substrates.....	37
Figure 4.5	Absorbance spectra of yellowish glass substrate before and after grinding .....	37
Figure 4.6	Overview of overall photovoltaic cell layers (a) with covered part before PLD (b) after PLD (c) before gold sputtering with mask (d) after gold sputtering .....	40
Figure 4.7	Illumination set-up .....	41
Figure 4.8	Circuit elements connection.....	41
Figure 4.9	Resistor effect on I-V curve .....	42
Figure 4.10	I-V curve of SP08 at illumination set-up .....	43
Figure 4.11	I-V curve of SP08 at various irradiance levels .....	43
Figure 4.12	Sample stage for thin film PVs, (left) front and (right) behind.....	44
Figure 4.13	Illustration of thin film photovoltaic cell under illumination .....	45
Figure 5.1	XRD patterns of FTO350 films .....	47
Figure 5.2	SEM image of TiO <sub>2</sub> film deposited on FTO at 350°C, 0.4 mbar oxygen pressure, with TiO <sub>2</sub> powder target.....	47
Figure 5.3	Optical transmission spectra of TiO <sub>2</sub> films deposited on FTO substrates.	48
Figure 5.4	Optical transmission spectra of FTO350 as-deposited and annealed films .....	49
Figure 5.5	Optical indirect band gap data of FTO350 as-deposited and annealed films .....	50
Figure 5.6	XRD of ITO005.....	51
Figure 5.7	XRD of ITO02.....	51
Figure 5.8	SEM images of TiO <sub>2</sub> films deposited on ITO (a) 0.05 mbar (b) 0.2 mbar oxygen pressure .....	52
Figure 5.9	Optical transmission spectra of ITO005 and ITO02 as-deposited films ....	53
Figure 5.10	Optical indirect band gap data of ITO005 and ITO02 films.....	54
Figure 5.11	XRD patterns of copper oxide films prepared at 400°C and different oxygen partial pressures.....	55
Figure 5.12	SEM image of copper oxide layer on TiO <sub>2</sub> deposited FTO substrate .....	55
Figure 5.13	Absorbance spectra of copper oxide films prepared at 400°C and different oxygen partial pressures.....	56
Figure 5.14	Optical direct band gap data of copper oxide, deposited under 2x10 <sup>-4</sup> mbar oxygen partial pressure and its absorbance spectra on the inset graph .....	57
Figure 5.15	Optical direct band gap data of copper oxide, deposited under without oxygen and 2x10 <sup>-2</sup> mbar oxygen partial pressure conditions.....	57
Figure 5.16	XRD pattern of photovoltaic cell .....	58
Figure 5.17	SEM image of photovoltaic cell .....	59
Figure 5.18	Absorption coefficient of copper oxide layer on PV, as comparison with sunlight .....	60

Figure 5.19	Optical direct band gap data of copper oxide layer on PV, and its absorbance spectra on the inset graph.....	60
Figure 5.20	Illustration for possible pathway of excited electron in the $\text{TiO}_2/\text{Cu}_2\text{O}$ heterojunction.....	61

## LIST OF TABLES

---

Table 2.1	Solar panel performance with increasing temperature [20] .....	18
Table 4.1	List the four types of layers in thin film solar cell together with their specific tasks and requirements necessary for an efficient solar cell[56] ..	34
Table 4.2	Illumination set-up components .....	41
Table 4.3	Comparison of silicon solar cell certified specifications and solar simulator set-up.....	43
Table 5.1	Sample structure and band gap of FTO350.....	50
Table 5.2	Sample structure and band gap of ITO samples.....	54
Table 5.3	Structure and band gap of copper oxide films .....	58

---

**CHARACTERIZATION OF TiO<sub>2</sub>/Cu<sub>2</sub>O THIN FILM PHOTOVOLTAIC CELLS**

Tülin YILMAZ

Department of Chemical Engineering

MSc. Thesis

Adviser: Prof.Dr.Hanifi Saraç

Photovoltaic cells (PVs) generate electricity by using sunlight. Although they have been known since years, they have recently been famous with increasing renewable energy demand. Nowadays, silicon solar cells are mostly used. But to achieve lower cost and improve manufacturing for large scale, different kind of PVs should be established. While PVs' demand grow, new materials should be supplied. In this perspective Cu<sub>2</sub>O is an attractive material as an absorber and TiO<sub>2</sub> is known as a large band gap semiconductor. When these two semiconductors are brought together, a p-n junction is created which is promising as a solar cell.

In this thesis, TiO<sub>2</sub>/Cu<sub>2</sub>O thin film PV characterization was studied. Characterization focused on optical properties of thin films as transmittance, absorbance, band gap values and behaviors under illumination related with their structural properties. Thin film deposition was processed by pulsed laser deposition method.

In the first part of the report, variable temperatures, pressures and transparent conductive layers were used to achieve anatase crystal phase for TiO<sub>2</sub> layer. Under 0.4 mbar oxygen pressure and 350°C, 450°C, 550°C temperatures, thin film samples were deposited on FTO substrates.

The XRD results showed that as-deposited films were amorphous so films were subjected to annealing process at 600°C and 650°C. After 600°C annealing, anatase phase was achieved and after 650°C annealing, anatase-rutile transformation was observed. Band gap values decreased after annealing; 3.45-3.29 -3.15 eV, respectively. Under 500°C deposition temperature and 0.05 mbar, 0.2 mbar oxygen pressures, thin films were deposited on ITO substrates. XRD results showed that as-deposited films

were anatase+rutile mixed phase and anatase phase, under these pressures. Band gaps were 3.28-3.33 eV respectively.

Second part was obtaining the Cu<sub>2</sub>O phase by adjusting the oxygen partial pressure. Under 0.2 mbar Ar atmosphere and  $2 \times 10^{-4}$  mbar- $2 \times 10^{-2}$  mbar oxygen partial pressures, samples were deposited on TiO<sub>2</sub> layers which were growth on FTO. Structure of films were changed from Cu<sub>2</sub>O to CuO with increasing oxygen partial pressures. Band gap values were estimated as 2.58, 2.58 and 2.07 eV with increasing oxygen partial pressures. Third part was applying the individual layer deposition parameters to overall photovoltaic cell. Overall PV structure was poor anatase and Cu<sub>2</sub>O phases. To investigate the electrical properties of photovoltaic cells, an illumination set-up was arranged. Set-up properties and sample response results under illumination were discussed in the results part.

**Key words:** Photovoltaic cells, semiconductor, p-n junction, thin film, transmittance, absorbance, band gap.

## TiO<sub>2</sub>/Cu<sub>2</sub>O İNCE FİLM FOTOVOLTAİK HÜCRELERİN KARAKTERİZASYONU

Tülin YILMAZ

Kimya Mühendisliği Bölümü

Yüksek Lisans Tezi

Tez Danışmanı: Prof.Dr.Hanifi Saraç

Fotovoltaik hücreler, güneş ışığını kullanarak elektrik enerjisi üretirler. Güneş hücreleri senelerdir biliniyor olmalarına rağmen, son zamanlarda artan enerji ihtiyacıyla birlikte daha sık gündeme gelmeye başlamışlardır. Günümüzde en sık kullanılan güneş hücreleri, silikon güneş hücreleridir. Üretim maliyetlerini düşürmek ve daha geniş alanlarda uygulanabilirliği arttırmak amacıyla yenilikçi malzemelerin belirlenmesi gereklidir. Bu anlamda, Cu<sub>2</sub>O, iyi absorplayıcı bir malzeme olma ve ucuz bir hammadde olma özellikleri ile güneş pilleri üretimi için öne çıkan bir malzemedir. TiO<sub>2</sub> ise geniş bant aralığı ile bilinen bir yarı iletkenidir. Cu<sub>2</sub>O ve TiO<sub>2</sub> biraraya getirildiğinde verimli güneş hücreleri üretimi için umut verici bir p-n eklemi elde edilir.

Bu tezde, TiO<sub>2</sub>/Cu<sub>2</sub>O ince film fotovoltaik hücre karakterizasyonu çalışılmıştır. Karakterizasyon, ince filmlerin geçirimsizlik, absorplama ve bant aralıkları gibi optik özellikleri ve ışık altındaki davranışlarını kapsamaktadır. İnce film üretimi için lazer biriktirme yöntemi kullanılmıştır. Çalışmanın ilk bölümünde, farklı sıcaklık, basınç ve transparan iletken tabaklar kullanılarak TiO<sub>2</sub> anataz kristalini elde etmek amaçlanmıştır. 0,4 mbar oksijen basıncı altında, 350°C, 450°C ve 550°C sıcaklıklarda FTO alt tabakası kullanılarak, TiO<sub>2</sub> ince filmleri üretilmiştir. XRD sonuçları, üretim sonrası filmlerin amorf olduğunu gösterdiğinden, örnekler 600°C ve 650°C'de ısıtılma tabii tutulmuştur. 600°C'de tavlama sonrası anataz elde edilirken, 650°C'de tavlama sonrası anataz-rutil faz dönüşümü görülmüştür. Bant aralığı değerlerinde tavlama ile azalma görülmüştür. Bant aralığı değerleri sırasıyla; 3,45-3,29-3,15 eV'dir. 500°C sıcaklıkta, 0,05 mbar ve 0,2 mbar oksijen basıncı altında ITO alt tabakalarına TiO<sub>2</sub> ince filmleri üretilmiştir. XRD sonuçları, üretim sonrası filmlerde anataz-rutil karışımı ve anataz fazının elde edildiğini göstermiştir. Bant aralığı değerleri bu basınçlarda sırasıyla;

3,28 eV ve 3,33 eV'dir. Çalışmanın ikinci bölümü, Cu<sub>2</sub>O'nun üretim sırasındaki kısmi oksijen basıncıyla etkilendiğini göstermektedir. Sadece 0,2 mbar Ar atmosferinde, 2x10<sup>-4</sup> mbar ve 2x10<sup>-2</sup> mbar oksijen kısmi basınçları altında üretim yapılmıştır. Film yapısının, artan kısmi oksijen basıncıyla, Cu<sub>2</sub>O'ten CuO'e değiştiği görülmüştür. Bant boşluğu değerleri, farklı basınçlar altında üretilen örnekler için sırasıyla; 2,58 eV, 2,58 eV ve 2,07 eV olarak tahmin edilmiştir. Çalışmanın üçüncü bölümü, ideal üretim koşulları ayrı ayrı belirlenen tabakaların, tam fotovoltaik hücreye uygulanmasını içermektedir. Tam fotovoltaik hücre yapısı, anataz ve Cu<sub>2</sub>O fazlarını içeren tabakalardan oluşmaktadır. Fotovoltaik hücrenin elektriksel özelliklerini saptamak için bir aydınlatma düzeneği kurulmuştur. Düzeneğin kurulum özellikleri ve hücrelerin ölçüm sonuçları, sonuçlar bölümünde tartışılmıştır.

**Anahtar kelimeler:** Fotovoltaik hücre, yarı iletken, p-n eklemi, ince film, geçirgenlik, absorban, bant aralığı.



### INTRODUCTION

#### 1.1 Literature Review

The idea of using renewable energy sources to overcome the energy resource problem is rewarding for society. New energy sources other than fossil fuels are needed for human beings to live in a healthy environment less threat for their future. Solar energy is a popular energy source in science nowadays. The possibility of creating a high end photovoltaic is valuable. The ambitious goals are interesting for scientists. In this way, solar cells will be future's fuel supplier.

The ninety minutes of sunlight energy is enough to provide entire planet one year energy needs [1]. Solar resource is enormous when compared to our energy needs. The sun offers a respectable amount of power; about 885 million terawatt-hours (TWh) reaches the earth's surface in a year, that is 6200 times the commercial primary energy consumed by humanity in 2008 and 4200 times the energy that humanity would consume in 2035 following the IEA's Current Policies Scenario [1]. While proven fossil reserves represent 46 years (oil), 58 years (natural gas) and almost 150 years (coal) of consumption at current rates, the energy received by the sun in one single year, if entirely captured and stored, would represent more than 6000 years of total energy consumption. Although the sun serves this large amount of energy and it has a huge part (Figure 1.1) between total energy sources, solar energy recently shows up in energy statistics.

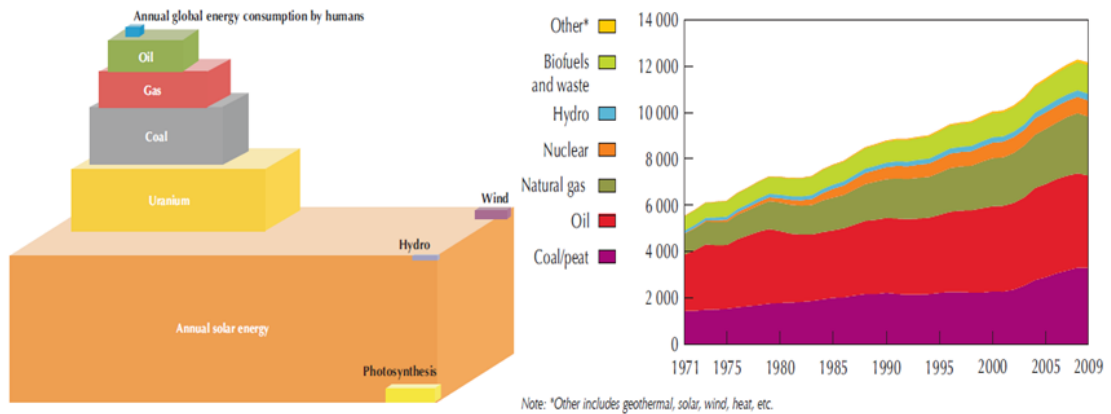


Figure 1.1 Total energy sources (left) and evolution of world total primary energy supply (Mtoe<sup>1</sup>) [1]

Solar technologies are generally characterized as active solar and passive solar their difference depends on the way of capturing, converting and distributing the solar energy. The orientation of buildings towards the south to capture the sunlight is a known sample for passive solar energy which collects the energy from sun. Active solar energy includes the photovoltaics and solar thermal which harvest from sunlight to store it or convert it other forms for other applications.

As one of the well-known solar technology photovoltaics are commonly abbreviated “PV”. The name implies that “photo” means light and “voltaic” means electricity. PV devices (solar cells) are developed as a method of capturing the sun’s energy and converting it to electricity.

PV technology has been known for many years, but its large scale use began only in the last few years. The increasing usage is also a result of increasing demands. In other words, people’s incline to the sun as a energy supplier increased the PV investments. The results of these investments can be seen on for example rooftops and handheld calculators.

Manufactured PV cells’ main part is semiconductor materials and they are also known from computer chips. When sunlight hit the cells, it is absorbed by semiconductor. Then the electrons flow through the cell and electricity generation occurs. This

<sup>1</sup> Tonne of oil equivalent, 1 toe = 11.63 megawatt hours

electron flow is a current which defines the solar cell's power with the cell's voltage. The conversion of energy that is absorbed from sun by the solar device indicates solar device's efficiency.

While photovoltaic cells present ease of operation as is mentioned above, their efficiency and cost relations are not satisfying. Maximum efficiency of a single junction solar cell can be obtained around 33.7% assuming that single junction band gap 1.34 eV, referring to Shockley-Queisser limit (detailed balance limit)[2]. This limit is related with the blackbody radiation, recombination of excited electrons and spectral losses. The limitation based on a single junction solar cell, one incoming photon excites only one electron and illumination under unconcentrated sunlight.

Silicon is the most popular solar cell material with its 1.1 eV band gap. According to Shockley-Queisser limit, its maximum theoretical efficiency can be 29%. Industrial silicon solar cells efficiency is between 18%-24%. However, silicon cells manufacturing cost is expensive. Thus, researchers are trended to find cheap and efficient solar device types. In this way, metal oxide (MO) semiconductors are very attractive to achieve low cost production processes; they are chemically stable and many of them are nontoxic. So, devices that made from semiconductors should provide important requirements for PVs which are inexpensive, chemically stable and environmentally safe, besides the conversion efficiency.

## **1.2 Objective of Thesis**

Metal oxides (MO) are widely used as components in PV cells such as transparent conducting front electrodes and light absorbers. While only few MOs have been used as light absorber,  $\text{Cu}_2\text{O}$  is one of the mostly used. However,  $\text{TiO}_2/\text{Cu}_2\text{O}$  p-n junction photovoltaic cell studies are not commonly used in the literature studies. Some of them which involve  $\text{TiO}_2/\text{Cu}_2\text{O}$  junction use different deposition techniques than the pulsed laser deposition (PLD). In this perspective, this project focuses on the characterization of  $\text{Cu}_2\text{O}$  photovoltaic cell which was fabricated by PLD. Layers of the solar cell from top (where the sunlight comes first) to bottom are a substrate ITO or FTO, a n-type semiconductor  $\text{TiO}_2$  and p-type semiconductor  $\text{Cu}_2\text{O}$ . Characterization depends on the optical measurements and photovoltaic inspection by an illumination

set-up. An illumination set-up was arranged to make operational a photoconductance tool in University of Twente ICE group laboratory.

### **1.3 Hypothesis**

New materials developing for the photovoltaic applications are very important topic for the researchers since silicon is expensive both as a raw material and in the PV manufacturing processes.  $\text{Cu}_2\text{O}$  is one of these materials for PVs. Its photovoltaic behavior with the some electron conductor materials is still investigated.  $\text{TiO}_2/\text{Cu}_2\text{O}$  junction exhibits promising system for solar cells. In this thesis, the structural and electrical behaviors find out for  $\text{TiO}_2/\text{Cu}_2\text{O}$  junction which is deposited by PLD is aimed.

This thesis involves that photovoltaic cell working principles and solar cell types in the trade and science in Chapter 2. In Chapter 3, mostly used fabrication technologies for the PV producing are explained. The experimental part of this work is described in Chapter 4 with pulsed laser deposition and illumination set-up. In Chapter 5, structural and optical results for every experiments are given. Finally, in Chapter 6, all results are summarized and recommendations are made.

PHOTOVOLTAIC TECHNOLOGY

The photovoltaic effect was first observed by Alexandre-Edmond Becquerel in 1839. The first patents for solar cells were reported in the 1920s by Walter Snelling and Walter Schottky. In 1954, Darryl Chapin, Calvin Fuller and Gerald Pearson, colleagues of Bell Labs, invented the silicon solar cell for powering satellite instruments. In the early 1970s, Elliot Berman adapted the PV to terrestrial applications. In the years 2005-2010 the global solar cell capacity made a jump from 5 GW to 40 GW.

While the world’s cumulative PV capacity is exceeding 100 GW in 2012(Figure 2.1), Europe is coming first in the photovoltaic market with 70 GW. Next in the ranking are China (8.3 GW) and the USA (7.8 GW) followed by Japan (6.9 GW) [3]. China, India and Latin America are growing fast in photovoltaics usage, because of local energy demand. In the Middle East region, Israel remains the only country with a significant market, while Saudi Arabia started to show some interest for PV development. The Turkish market remains quite low despite its potential (Figure 2.2).

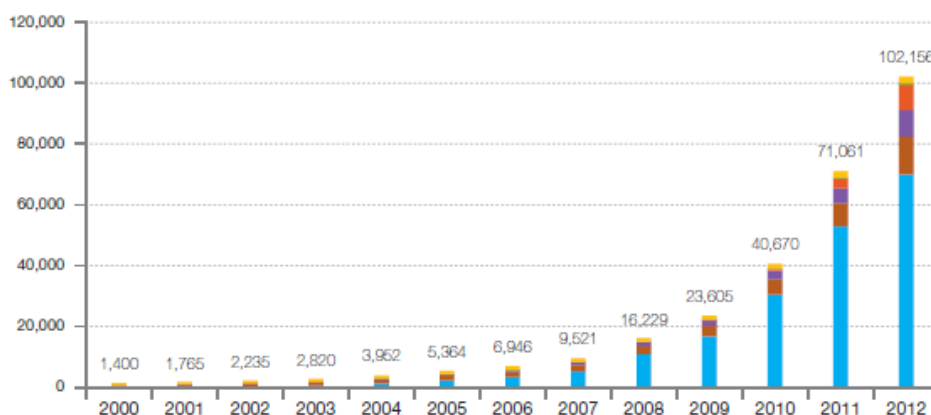


Figure 2.1 Evolution of global PV cumulative installed capacity 2000-2012 (GW) [3]

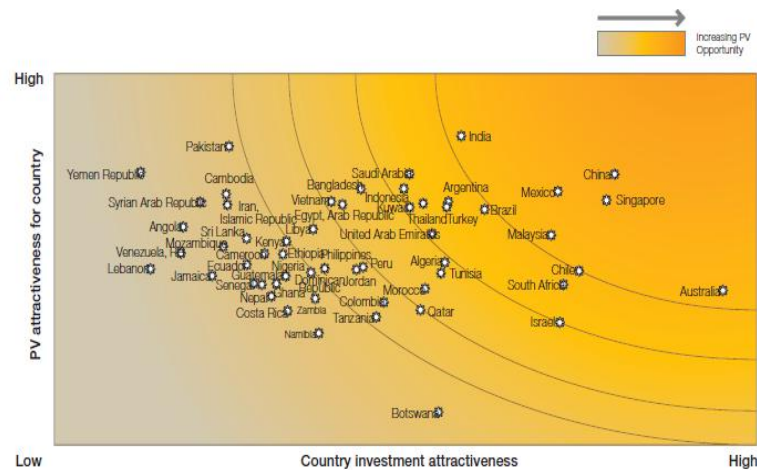


Figure 2.2 PV Opportunity mapping of sunbelt countries [3]

## 2.1 Photovoltaic Effect

Photovoltaic effect can be defined as a generation of a electromotive force or potential by the absorption of light in a semiconductor[4], [5].

When sunlight falls on the solar device, the photons are absorbed and promote an electron from valence band to conduction band as leaving a hole behind. Therefore electron-hole pair is generated. For absorption, the minimum energy of a photon must be larger than the *band gap* of the absorbing material. Electron-hole pairs are separated by the *junction* to allow the minority carriers to reach a region which they are the majority. Then they transport to contacts to process the photocurrent. The type of *majority and minority carriers* depends on the type of semiconductor, *p-type* or *n-type*. This definition summarizes how a solar device works. To understand this mechanism, we need to know more explanations. Therefore paper will continue through these explanations.

### 2.1.1 Band Gap

The band gap is the minimum amount of energy required for an electron to breaks its bound state. In other words, band gap is the energy between valance band ( $E_V$ ) and conduction band ( $E_C$ ). A *valence band (VB)* in which they are bound to atoms, and a *conduction band (CB)* in which they are free to move around in the solid. The conduction band is at a higher energy level than the valence band, but in a conductor

the top of the valence band overlaps with the bottom of the conduction band, as shown in Figure 2.3[6].

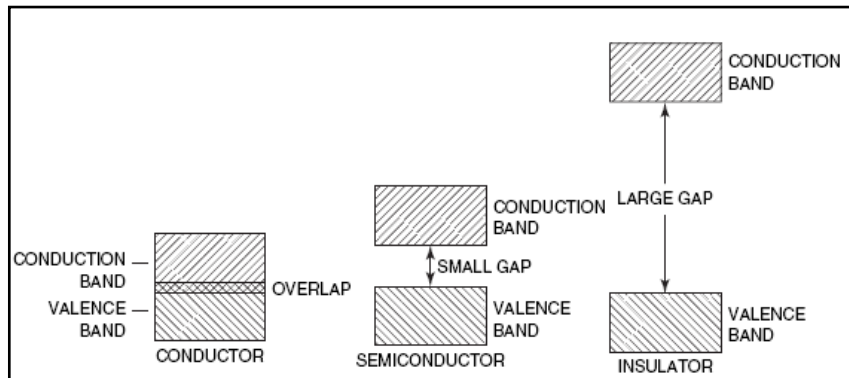


Figure 2.3 VB and CB in conductor, semiconductor and insulator [6]

The band gap can be classified as direct or indirect band gap which are determined according to alignment of valence and conduction bands. Valence band and conduction bands are both characterized by certain crystal momentum ( $k$  vector). If the energy minimum (the bottom) of the conduction band has same crystal momentum value with the energy maximum (the top) of the valence band, which means that valence band top side directly lies under the conduction band bottom side, it is called "direct"; otherwise, it is called "indirect" band gap [7], [8].

While an electron can directly discharge from a semiconductor which has direct band gap, in an indirect gap semiconductor, this can not happen directly because the electron must pass through an intermediate state and transfer momentum to the crystal lattice. Direct and indirect band gap is shown Figure 2.4.

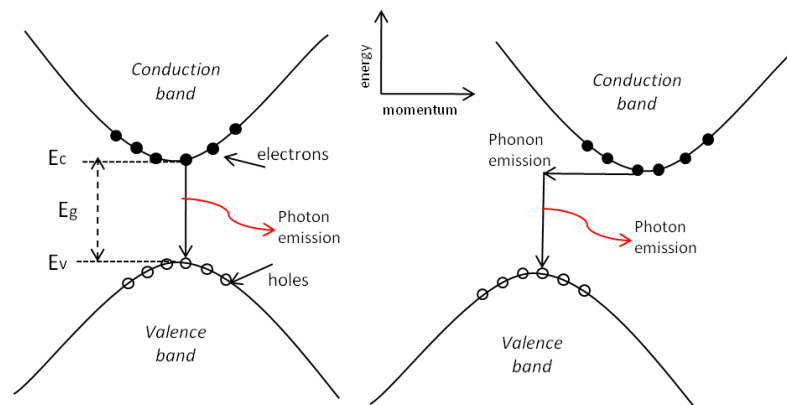


Figure 2.4 Conduction and valence band positions for direct (left) and indirect (right) band gap

The band gap energy,  $E_g$ , can be calculated by plotting according to Tauc expression (2.1) [9].

$$\alpha h\nu = A_f (h\nu - E_g)^n \quad (2.1)$$

In Equation (2.1),  $h\nu$  is the incident photon energy,  $A_f$  is a proportional constant which doesn't depend on photon energy and  $n$  depends on the transition type.  $n=1/2$  for direct transitions and  $n=2$  for indirect transitions. In the graph of  $(\alpha \cdot h\nu)^{1/n}$  versus photon energy ( $h\nu$ ), if the linear part is extrapolated to point that  $(\alpha \cdot h\nu)^{1/n} = 0$ ,  $E_g$  is estimated at this point.

Absorption,  $\alpha$  is calculated with using equation (2.2) [10], where  $d$  is film thickness and  $T$  is film transparency.

$$\alpha = d^{-1} \ln\left(\frac{1}{T}\right) \quad (2.2)$$

Sunlight, as all electromagnetic radiation, consisted on the particles which are called photons. Photons have a specific energy values according to spectral properties. So their energies are calculated with the relation to the wavelength[8]. Photon energy equation is given in equation (2.3).

$$E_\lambda = \frac{hc}{\lambda} \quad (2.3)$$

In equation (2.3)  $h$  is plank constant ( $6.626 \times 10^{-34}$  kg m<sup>2</sup>/sec),  $c$  is light speed ( $3 \times 10^8$  m/sec),  $\lambda$  is wavelenght and 1eV equals to  $1.6 \times 10^{-19}$  Joules.

In order for a photon to be absorbed the minimum energy of it should be equal or larger than the bandgap. Therefore  $E_\lambda$  should be greater than  $E_g$ .

### 2.1.2 Doping

It is possible to change the balance of electrons and holes in a semiconductor. This is by adding other atoms in the crystal lattice. This technique is called doping.

A semiconductor either *p-type* or *n-type* is determined by donating atom. If an atom contributes its electrons to a semiconductor to create free negative carriers is called *n-type*. On the other hand, if a semiconductor is doped with atoms that produce holes (or electron acceptors) is called *p-type* and it contains extra holes as positive current carriers. Undoped semiconductors are called *intrinsic* or *i-type* [6].



Figure 2.5 [11] illustrates n-type and p-type silicon. Because of silicon is the mostly used semiconductor, many doping experience's figures are illustrated around it. On the Figure 2.5, n-type silicon was created by antimony doping and p-type silicon was created by boron doping. Silicon has four valence electrons. Antimony has five valence electrons. When an antimony atom is added silicon crystal lattice, its four electrons form covalent bonds around the silicon so an extra valence electron will be available to slide through the semiconductor. During the boron doping, its only three electrons interact with silicon's valence electrons so this is resulted with a hole.

In doped material, there is always one type of carrier more than the other and the type of carrier with the higher concentration is called a "majority carrier", while the lower concentration carrier is called a "minority carrier" [12].

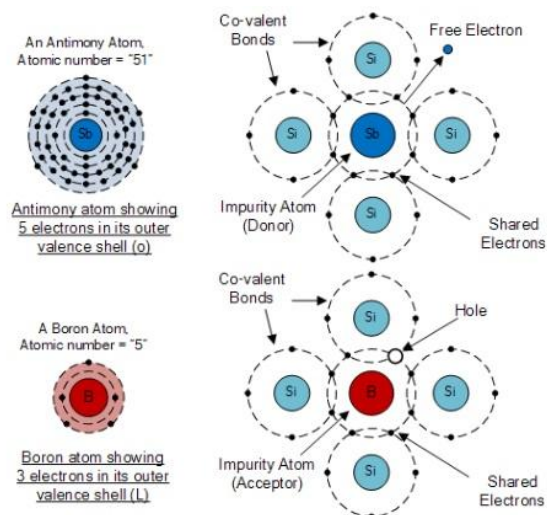


Figure 2.5 n-type silicon (top) and p-type silicon (bottom) by doping [11]

### 2.1.3 Semiconductor materials

A semiconductor can be defined by its different features from conductor or insulator. Most used definition is that a semiconductor material which has an electrical conductivity to a degree between a conductor and an insulator.

Semiconductors (e.g.,  $\text{TiO}_2$ ,  $\text{ZnO}$ ,  $\text{Fe}_2\text{O}_3$ ,  $\text{CdS}$ , and  $\text{ZnS}$ ) are light sensitive materials due to their electronic band structure, which is characterized by a filled valence band and an empty conduction band [13].

When n-type semiconductor and p-type semiconductor are brought together, electrons and holes diffusion will start. Electrons which are majority carriers in the n-type material diffuse to the p-type material. Holes which are majority carriers for p-type material will diffuse to the n-type side. If the electrons and holes aren't charged, this diffusion will continue until the electrons and holes concentration in both side will be same. However, when electrons go towards the p-type side, they leave behind positive ion cores and when holes accross towards the n-type side, they leave negative ion cores. Therefore an **internal electric field ( $E$ )** forms at the junction. This region is called the "**depletion region**" since internal electric field sweeps carriers out, this region is depleted of free carriers. Regions outside the depletion region is called "quasi-neutral regions".

Electrons, holes diffusion and depletion region is illustrated on Figure 2.6.

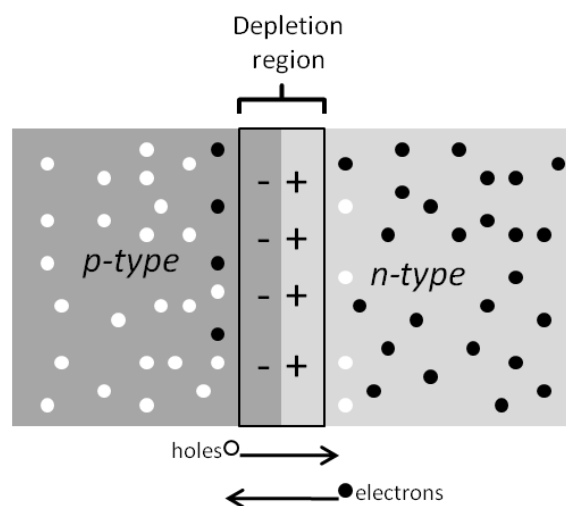


Figure 2.6 Diffusion and depletion region in p-n junction

The depletion region is highly resistive because it doesn't have mobile carriers. Resistance of the depletion region can be changed by applying voltage to p-n junction. Under reverse bias which means applying a positive voltage to the n side of junction and a negative voltage to the p-side, carriers are directed away from the junction since the depletion region becomes wider and more resistive. Therefore no current flows through the junction. If a diode is forward biased which means applying a positive voltage to the p side and a negative voltage to the n side, this attracts the holes to the n-side and electrons to the p-side since the depletion region becomes narrower, resistance is very smaller.

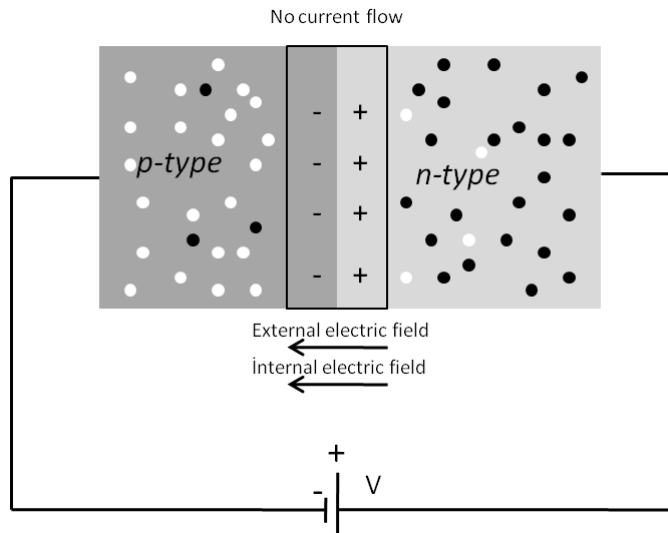


Figure 2.7 p-n junction under reverse bias

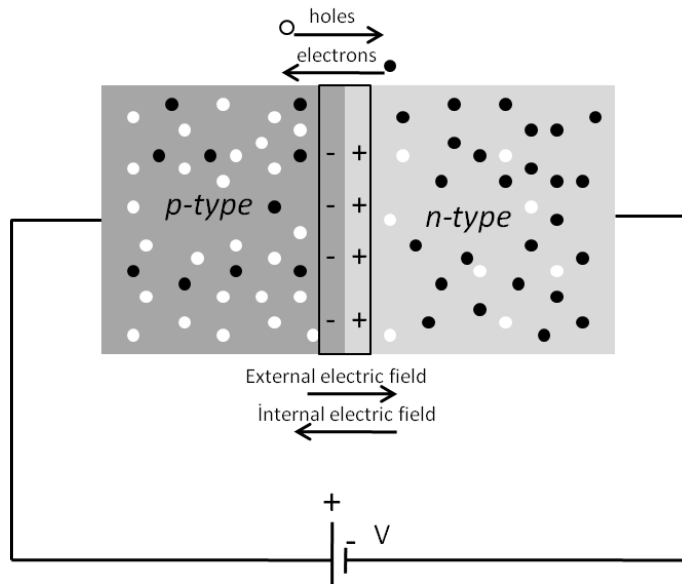


Figure 2.8 p-n junction under forward bias

When a photon with an energy that is equal or more than the band gap energy ( $E_g$ ) of the semiconductor is absorbed, an electron is promoted from the valence band (VB), into the conduction band (CB), leaving a hole. Materials tend to return their equilibrium conditions so the excited electrons eventually go back to their original position. This is called **recombination**. An average time which a carrier can spend in an excited state before it recombines, is called **lifetime** and the distance which it can move from point of generation until recombination, is called **diffusion length**. Diffusion length and lifetime are important indicators for the efficient solar cells.

If the electrons and holes do not recombine and they transport to the external contacts, electrical current is generated.

## 2.2 Photovoltaic Characterization

Characterization equations are derived for diodes. But they are also used for photovoltaic cell characterization. A fundamental equation for microelectronics is Shockley equation which describes the behavior of an ideal p-n diode [14]:

$$I(V_a) = I_0 \exp\left(\frac{qV_a}{kT}\right) - 1 \quad (2.4)$$

At equation (2.4)  $I$  is expressed as the net current and it is as a function of applied voltage  $V_a$ .  $I_0$  represents the saturation current density of the p-n junction and it is determined by thermally generated minority carriers in the doped regions. Moreover,  $k$  is the Boltzman constant;  $q$  is the charge of an electron and  $T$  the temperature. Shockley equation consists of two physical parts: exponential part represents recombination current which occurs by diffusion of minority carriers into the quasi neutral region. The other part represents thermal generation current which is caused by the drift of minority carriers in the corresponding doped regions (electrons in the p-type region go through the n type and vice versa for holes in n-type region). While the net current flows through the p-n junction under forward bias voltage, under reverse bias voltage the Boltzman factor becomes very small and can be neglected. So  $I(V_a)$  will be equal to the  $-I_0$  [14]. The I-V characteristic of an ideal diode is given Figure 2.9.

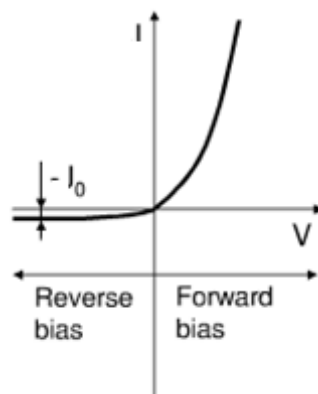


Figure 2.9 I-V characteristic of a p-n junction [14]

Under illumination of a p-n junction, electron-hole pair generation directs electrons from the p-type to the n type region and holes from the n-type to the p-type region.

These *photo-generated carriers* flow causes the **photo-generation current,  $I_{ph}$** . If there is not an external contact between the n type and p type regions, with other words the junction is in the open circuit condition, no net current flow inside the p-n junction. At this condition, a voltage difference can be measured between the terminals of the solar cell as **open circuit voltage,  $V_{oc}$** . If the terminals of the solar cell are short circuited and current flows through the external circuit this current is called as the **short circuit current,  $I_{sc}$** . The  $V_{oc}$  and  $I_{sc}$  represent the performance of solar cells.

If a voltage is applied between the electrodes of the illuminated p-n junction, photo generated current and external current flow opposite ways of the circuit. The net current flowing through the circuit is sum of photo-current, thermal current and recombination current [14]. So equation (2.4) should be written again addition with photo-current (2.5).

$$I(V_a) = I_0 \left[ \exp\left(\frac{qV_a}{kT}\right) - 1 \right] - I_{ph} \quad (2.5)$$

The dark and illuminated I-V characteristics of a p-n junction are represented Figure 2.10. In this figure red line shows maximum power point and blue line shows photo generation current.

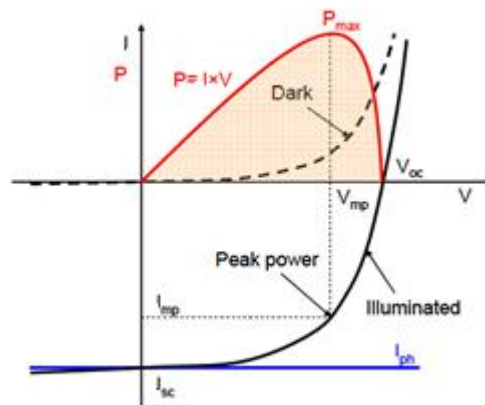


Figure 2.10 I-V characteristic of a p-n junction in the dark and under illumination [14]

The I-V curves are usually used to determine and understand the basic parameters of a device and can also be used to mathematically model its behavior in an electrical circuit. Peak power,  $P_{max}$ , short circuit current,  $I_{sc}$ , open circuit voltage,  $V_{oc}$ , and fill factor,  $FF$  are main parameters for characterization of a solar cell. Using these parameters, conversion efficiency,  $\eta$  is calculated. Maximum current and voltage are

obtained from the I-V curves by perpendiculars from maximum power point to abscissa and ordinate.

Fill factor (2.6) is the ratio between maximum power generated from solar cell and product of  $V_{oc}$  and  $I_{sc}$ :

$$FF = \frac{V_{mp} I_{mp}}{V_{oc} I_{sc}} \quad (2.6)$$

The conversion efficiency (2.7) is calculated as the ratio between the generated maximum power and the incident power:

$$\eta = \frac{P_{max}}{P_{in}} = \frac{V_{mp} I_{mp}}{P_{in}} = \frac{V_{oc} I_{sc} FF}{P_{in}} \quad (2.7)$$

The irradiance value,  $P_{in}$  is calculated with using area of solar cell and irradiance of light source. AM1.5,  $1000\text{W}/\text{m}^2$  has become a standard conditions for efficiency measurements.

### 2.3 Spectral Nature of Sunlight

Sunlight reaches the earth from approximately 93 million miles away by radiation. But for practical usage it is easier to think that sun strikes earth with direct photons which have different incident angles at different positions of sun [8]. Sunlight power reduces while it is taking way in the atmosphere. It absorbs air and dust through this way so its properties change. To characterize and standardize sun spectrum the *air mass coefficient* term is used with syntax AM. It is path length of the sunlight, given at equation (2.8) [8],[12].

$$AM = 1/\cos\theta \quad (2.8)$$

At equation (2.8)  $\theta$  is the angle from sun to zenith. While sun directly overhead the earth  $\theta$  is zero and AM1. On the earth surface air mass is equal to one or greater than one.

In photovoltaic researches, to compare all different solar cells experiments accurately, standard conditions were defined in 1980 based on AM1.5. From the calculation irradiance power is normalized as  $1000\text{ W}/\text{m}^2$ . According to this standard  $\theta=48.2$ .

Although zenith angle changes during a year, 48.2 is the useful for the overall yearly average [15].

The geometric conditions for standardization are given Figure 2.11. The receiving surface has been represented for the USA so that 37° tilted surface was selected to present average latitude of the USA [15].

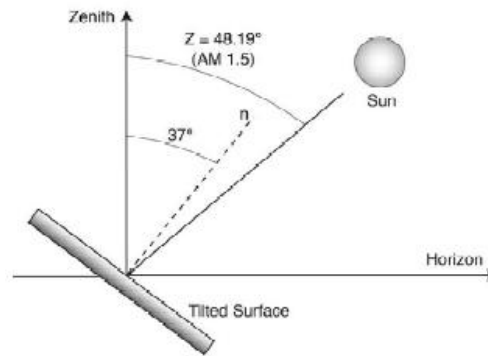


Figure 2.11 Standard spectral geometry [15]

## 2.4 Classification of Solar Cells

Solar cells can be classified in different groups which depend on materials, industrial usage and fabrication techniques.

General classification related to p-n junction type. If materials in each side of junction are same semiconductor but only different thing is doping method, this solar cell is called homojunction solar cell. If semiconductor materials are both different in each side of junction, this is called heterojunction solar cell. For instance,  $\text{SnO}_2/\text{CuInSe}_2$ ,  $\text{CdS}/\text{Cu}_2\text{S}$ ,  $\text{ZnO}/\text{Cu}_2\text{S}$  are heterojunction solar cells.

The other classification can be related with which solar cells are being used in industry and which are emerging with pre-industrial research techniques currently.

### 2.4.1 Industrial solar cells

These solar cells can be divided three main parts which are related with commonly used materials: Crystalline silicon solar cells, thin film solar cells and multijunction solar cells.

- **Crystalline silicon solar cells**

Silicon solar cells are called first generation solar cells. They date back more than 50 years to the early 1940s [16]. Throughout the decades, many research groups have contributed to improve device structures and methods for formation.

First silicon cell was made by Russel Ohl in 1946, from natural junction but with efficiencies well below 1%. After that, in 1954 The first practical photovoltaic cell was developed at Bell Laboratories by Daryl Chapin, Calvin Souther Fuller and Gerald Pearson. They used a diffused silicon p-n junction that reached 6% efficiency. From 1954 to 1960 Less Hoffman improved the efficiency of solar cells to 14%. At first, cells were developed for toys and other minor uses, as the cost of the electricity they produced was very high; in relative terms, a cell that produced 1 watt of electrical power in bright sunlight cost about \$250, comparing to \$2 to \$3 per watt for a coal plant [17].

The price of solar panels fell steadily for 40 years, until 2004, increased demand in Germany caused price increasing of purified silicon (which is used in computer chips as well as solar panels). Four years later in 2008, lead by Chinese manufacturing, prices for solar modules in Germany dropped from €3 to €1 per peak watt. During the same time production capacity surged with an annual growth of more than 50%. China increased market share from 8% in 2008 to over 55% in the last quarter of 2010 [17]. Recently, in December 2012 the price of Chinese solar panels had dropped to \$0.60/Wp (crystalline modules) [18].

Crystalline silicon is common bulk material for solar cells and it is separated into multiple categories according to crystallinity and crystal size in the resulting ingot, ribbon and wafer. These are listed in two main types; monocrystalline and polycrystalline which are entirely based around the concept of a p-n junction.

Monocrystalline wafer cells tend to be expensive because they are cut from cylindrical ingots so the crystalline framework is homogenous. Polycrystalline silicons are made from cast square ingots large blocks of molten silicon and they contain smaller crystals. These cells are less expensive than single crystal silicon cells to produce, but are less efficient.



As the most common solar cells used in commercially available solar cells, crystalline silicon PV cells are representing 87% of world PV cell market sales in 2011. Crystalline silicon PV cells have laboratory energy conversion efficiencies as high as 25% for monocrystalline cells and 20.4% for polycrystalline cells. However, industrially produced solar modules currently achieve 18%-24% efficiencies [19]. Figure 2.12 shows the appearance difference between mono and polycrystalline silicon solar cells.

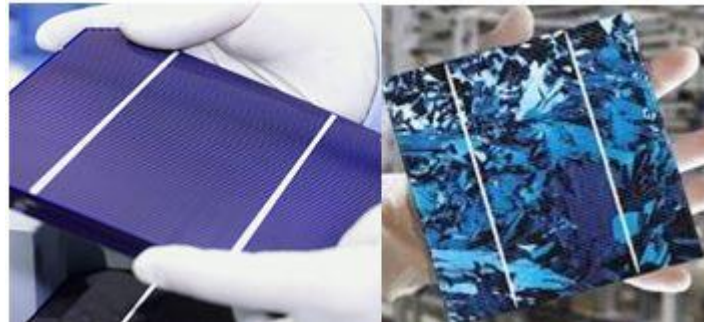


Figure 2.12 Monocrystalline silicon solar cell (left) and polycrystalline silicon solar cell (right)

- **Thin film technologies**

Thin film solar cell is made by depositing one or more thin layers of various photovoltaic (PV) materials on a substrate. The PV materials are carefully chosen to absorb a broader range of the solar spectrum that extends beyond visible light. Compared with the crystalline solar modules thin film modules are less efficient, at 8%-13% but they have a major advantage about the cost. Thin film panels cost approximately 30% less than crystalline panels (\$0.75 per watt)[20].

However, lower cost advantage makes thin film panel more attractive, they have other important features different from crystallines: flexibility and better performance in hot weather. While crystalline solar panel cells are 0.15-0.2 mm thick, thin film cells can be as thin as 0.001 mm so this makes them more flexible for installation. Temperature comparison is seen Table 2.1 [21], [22]. The electricity performance of photovoltaic module is measured by standard condition (STC) which include strong light (1000 W/m<sup>2</sup>, 1.5 AM solar spectrum) and 25°C solar cell temperature. However while operating under sunlight the temperature of solar module can be higher than atmosphere temperature 25°C, for roof of building installations 55°C is not unusual

temperature. In this case temperature coefficient is very important parameter for various solar cell technology. The temperature coefficient is usually minus and according to Ample-Sun's research, it is  $-0.2\%/^{\circ}\text{C}$  for thin films and  $-0.5\%/^{\circ}\text{C}$  for crystalline solar cell. That means, when module worked on  $50^{\circ}\text{C}$ , if we compare with the  $25^{\circ}\text{C}$  conditions, for thin films efficiency will loose 5% and 12.5% for crystalline [23].

Table 2.1 Solar panel performance with increasing temperature [20]

Temperature $^{\circ}\text{C}$	Efficiency of solar panel (%)	
	<i>a-Si thin film</i>	<i>Crystalline</i>
25 (STC)	10	16
35	8	11
45	6	6
50	5	3.5

Cadmium telluride (CdTe), copper indium gallium selenide (CIGS) and amorphous silicon (a-Si) are three thin film technologies which are often used in solar power production.

CdTe cells (Figure 2.13) are made of cadmium and tellurium. According to First Solar announcement in February 2013 which is an American manufacturer of thin film photovoltaic, cadmium telluride thin film solar cell efficiency world record was breaking. This solar cell efficiency is published as 18.7%. Its previous world record, in 2011 was 17.3% efficiency [24].

Amorphous silicon which is known from solar rechargeable calculators is the first thin film material available commercially. CIGS just recently became available for small commercial applications. Manufacturing is still expensive, but high efficiency in the lab has been achieved in 2013 as 20.4% by Swiss Federal Laboratories for Materials Science and Technology, EMPA [25].

- **Multijunction solar cells**

Multijunction cells currently used effectively with terrestrial solar concentrators. They were originally developed for special applications for instance, satellites and space exploration.

These solar cells include multiple p-n junctions that made of different semiconductor materials. For this reason each material's p-n junction response to a different wavelength of light so cell produce efficiently electric current at these different wavelengths.

Multijunction cells consist of multiple thin films for example a triple-junction cell consists GaAs, Ge and GaInP<sub>2</sub>. Combinations of semiconductors are very important for the efficiently absorption of sunlight. The world record for energy efficiency of a production solar cell had broken, in 2013, by The Fraunhofer Institute for Solar Energy Systems ISE, Soitec, CEA-Leti and the Helmholtz Center Berlin, with 44.7% rate of conversion of sunlight to electrical energy with four-junction cell [26]. Figure 2.13 shows this multijunction solar cell.

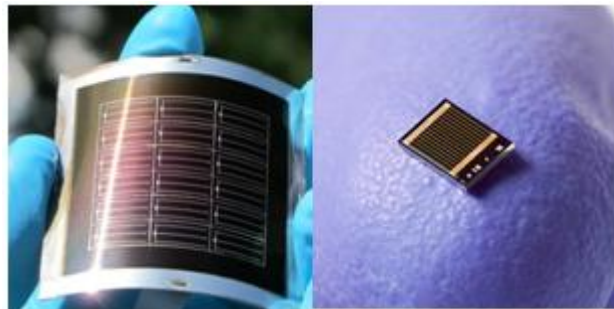


Figure 2.13 CdTe thin film solar cell (left), record-holder multi- junction solar cell (right)

#### 2.4.2 Pre-Industrial solar cells

The photovoltaic market has shown growth over the last years. Even though PV sector is exploding, PV generated electricity in most places are not compete in price with conventionally generated electricity. For this reason, new production processes are focused on cheap materials and deposition methods. Metal oxides, dyes and polymers (organic) are very popular materials for PVs as cheap production materials.

- ***Dye sensitized solar cells (DSSC)***

DSSC were published by O'Regan and Gratzel first time so these type of cells are also called "Gratzel cells". As explanation in their paper, dye sensitized solar cells separate the function of light absorption from charge carrier transport that differs them other cells. In the case of n-type materials, such as TiO<sub>2</sub> current is generated when a photon absorbed by a dye molecule gives rise to electron injection into the conduction band of

semiconductor. To complete the circuit, the dye must be regenerated by electron transfer from redox species in solution which is then reduced at the counter electrode [27]. Figure 2.14 illustrates schematic representation of this principle. The device was deposited with a monolayer of trimeric ruthenium complex harvests as an absorber layer. The overall light to electricity energy conversion yield is 7.1-7.9% in simulated solar light [27].

For years many experiments are experienced with different kind of dyes and semiconductors last one of them reached 33.2% efficiency with fabrication of Muscovite/TiO<sub>2</sub>/Dye/Al sandwiched photovoltaic cell. Solar cell was fabricated by using the technique of physical vapor deposition (PVD) and absorber dye was Rhodamine B [28].

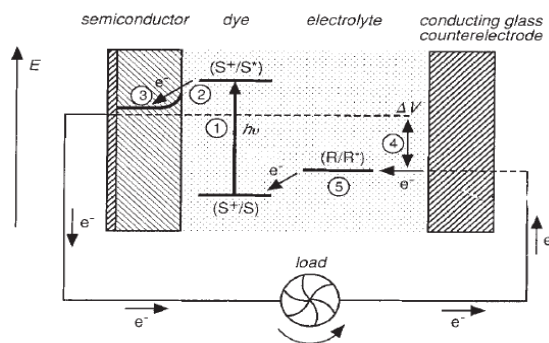


Figure 2.14 Principle of dye sensitized photovoltaic cell (S:Sensitizer, S<sup>\*</sup>:electronically excited sensitizer, S<sup>+</sup>: oxidized sensitizer)[27]

- **Polymer solar cells**

Polymer solar cells are built from thin films of semiconductors which includes polymer such as polyphenylene vinylene. Energy conversion efficiencies are very low compared to inorganic materials. One of the recent researchs has been demonstrated by Konarka Technologies to have 8.3% efficiency in 2010 and the cell was certified by the National Energy Renewable Laboratory as a new world record for an organic photovoltaic solar cell [29].

- **Metal oxide solar cells**

Metal oxides (MO) are commonly used in PV cells as transparent conducting oxides (TCO) for instance; fluorine doped thin oxide (FTO), indium tin oxide (ITO) or aluminum doped zinc oxide (AZO). Even though MO are widely used in PV cells only few MOs have been used as light absorbers.

Cu<sub>2</sub>O is a popular material for metal oxide solar cells. Its electronic band gap approximately 2.0 eV [30]. There are many reports on metal semiconductor heterojunction solar cells fabricated using Cu<sub>2</sub>O as the active layer but efficiency above 1% has been difficult. First maximum efficiency for Cu<sub>2</sub>O based solar cells is reported for Cu-Cu<sub>2</sub>O solar cell with 1.76% in 1981 [31]. After this report new maximum efficiency was recorded by AZO/ZO/Cu<sub>2</sub>O n-p heterojunction solar cell with 3.83% in 2011 [32].

Some of the new results for copper oxide based thin film solar cells will be given by chronological order.

Cu<sub>2</sub>O was grown electrochemically within TiO<sub>2</sub> films, nanotubes but the conversion efficiency remained below 1%. Lie et al. (2010) fabricated core-shell Cu<sub>2</sub>O/TiO<sub>2</sub> radial p-n heterojunction photovoltaic device by using electrodeposition method with an efficiency of 0.01% [33]. This experiment can be seen on Figure 2.15.

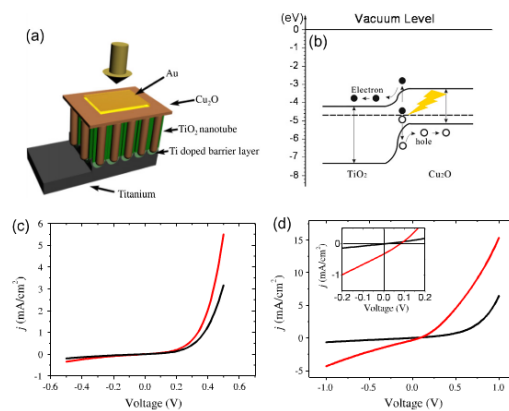


Figure 2.15 (a) Schematic diagram of Cu<sub>2</sub>O/TiO<sub>2</sub> core shell p-n junction photovoltaic, (b) Energy band diagram of Cu<sub>2</sub>O/TiO<sub>2</sub> p-n junction, (c) J-V characteristics before and (d) after annealing in Ar at 200° C for 1 h [33]

Musselman et al.(2010) [34] used electrodepositing to synthesize Cu<sub>2</sub>O/ZnO nanowire heterojunction solar cell. It showed 0.36% conversion efficiency. Nanowire arrays were grown on Zn seed layers on indium oxide (ITO)/ glass substrates and top contact Au was evaporated.

Another report was recorded 0.15% power conversion efficiency with p-Cu<sub>2</sub>O/n-TiO<sub>2</sub> thin film heterojunction solar cells by Hussain et al. (2012) [35]. Fabrication was processed on two steps, radio frequency (rf) magnetron sputtering of TiO<sub>2</sub> followed by electrodeposition of Cu<sub>2</sub>O. TiO<sub>2</sub> layers were deposited on a indium tin oxide (ITO) coated glass substrate. Figure 2.16 illustrates the results of this report on the left side with energy level band diagram of heterojunction solar cell with the energy band gap of Cu<sub>2</sub>O and TiO<sub>2</sub> and on the right side the current-voltage characteristics of cell in dark and under illumination, the inset shows the ohmic behaviour between Cu<sub>2</sub>O and TiO<sub>2</sub>.

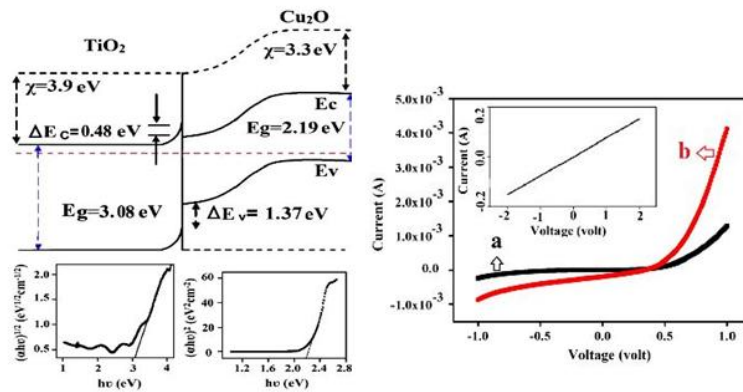


Figure 2.16 (left) Energy level band diagram, (right) the current-voltage characteristics of the Cu<sub>2</sub>O/TiO<sub>2</sub> thin film (a) in the dark (b) under illumination [35]

Chen et al. (2012) reported on fabrication of IZO/Cu<sub>2</sub>O heterostructure solar cells in which the Cu<sub>2</sub>O layers were prepared by oxidation of Cu thin films deposited on glass substrate [36]. One micron thick cuprous oxide film is deposited by magnetron reactive sputtering. Indium oxide doped zinc oxide (IZO) was deposited onto the Cu<sub>2</sub>O layer by sputtering and indium electrodes were formed by the evaporation onto both the surface of the IZO layer and the Cu<sub>2</sub>O layer (Figure 2.17). The measured parameters of

solar cells were short circuit current, the open circuit voltage, the fill factor, and the efficiency, which had values of 0.11 mA, 0.136 V, 0.338 and 0.56% respectively.

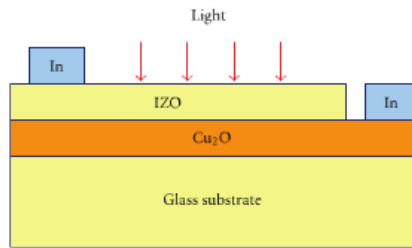


Figure 2.17 Schematic cross-section of the completed structure[36]

Kidowaki et al.(2012) used another form of copper, CuO, as an active layer for a photovoltaic device. It based on an ITO/CuO/C<sub>60</sub> heterojunction structure by the spin coated method. Finally,  $1.8 \times 10^{-6}$  % efficiency provided with 3.7 eV band gap of CuO which is higher than the typically in literature reported band gap of CuO [37].

Rühle et al.(2012) [30] have recently developed an all oxide bilayer heterojunction cells to bring all-oxide PV with using CuO and Co<sub>3</sub>O<sub>4</sub> as light absorbers. PV cells contains as a substrate, FTO and TiO<sub>2</sub> layer on it which was deposited by spray pyrolysis, followed by CuO or Co<sub>3</sub>O<sub>4</sub> absorber layer deposition by pulsed laser deposition. For back contact Cr and Au layers were sputtered. For TiO<sub>2</sub>/CuO and TiO<sub>2</sub>/Co<sub>3</sub>O<sub>4</sub> bilayer heterojunctions I-V curves measured and conversion efficiency stayed far below 1%.

p-Cu<sub>2</sub>O/n-ZnO nanowires were fabricated on ITO/glass substrates by Baek et al.(2013)[38]. The Cu<sub>2</sub>O was electrodeposited as the absorber layer, the ZnO film was formed on the ITO as an electron injection layer. To fabricate Cu<sub>2</sub>O/ZnO nanowire structure the Al doped ZnO (AZO) layer was deposited by atomic layer deposition (ALD) on ITO substrate for the vertical alignment of ZnO nanowire arrays. The conversion efficiency of this structure was 0.27% under 1.5 AM illumination.

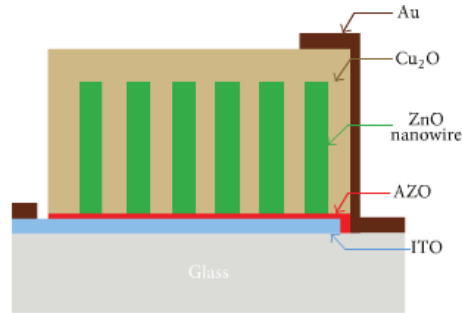


Figure 2.18 Schematic drawing of the Au/Cu<sub>2</sub>O/ZnO nanowires/AZO/ITO/glass heterostructure solar cell [38]

Rühle et al.(2014)[39] studied TiO<sub>2</sub>-Cu<sub>2</sub>O heterojunction solar cells on FTO substrate with different back contacts; Au, ITO, Cu and Ag. They produced linear TiO<sub>2</sub> thickness gradient using spray pyrolysis and a bell shaped Cu<sub>2</sub>O profile using Pulsed laser deposition. They aim to investigate metal oxide layers with different thickness. They patched 169 back contact for each of them so totally 676 contacts were patched on a solar cell library. Each contact represented a solar cell with different TiO<sub>2</sub> and Cu<sub>2</sub>O layer thicknesses. Cu<sub>2</sub>O band gap was estimated 2.5 eV for all library. They showed that open circuit voltage of TiO<sub>2</sub>-Cu<sub>2</sub>O heterojunction solar cells is approximately 300 mV and it is independent of the metal oxide layers thicknesses and metal contact type.



### FABRICATION OF THIN FILMS FOR PHOTOVOLTAIC APPLICATIONS

A thin film is a layer of material which is created by growth processes on a substrate. Thin films may involve thickness range, varying from a few nanometers (monolayer) to several micrometers. The structural, chemical and physical properties of thin film materials are mainly dependent on the deposition parameters.

Thin film deposition is defined as the applying a thin film to a surface. Although “thin” is a relative term, most deposition techniques control layer thickness within a few tens of nanometers. Deposition techniques fall into two main categories as chemical deposition and physical deposition.

Although physical deposition methods are used in this work, other deposition methods are also explained briefly.

#### 3.1 Chemical Deposition

In this technique, a fluid precursor undergoes a chemical change at a solid surface, leaving a solid layer. Deposition can be occurred any surface since the fluid surround the solid object. Chemical deposition techniques can be categorized by the phase of precursor. Chemical solution deposition, spin coating and chemical vapor deposition are mostly used chemical deposition techniques for thin film applications.

##### 3.1.1 Chemical solution deposition

Chemical solution deposition (CSD) is also known “sol-gel” technique because of solution evolve towards the formation of a gel. The process starts with the preparation

of precursors as carboxylates or metallo-organic compounds, usually, alkoxides. The precursors are dissolved in appropriate solvents and mixed in a stoichiometric ratio that yields the desired composition of the thin film. The next processing step is deposition of the coating solution on the substrate by spin coating using a rotating substrate, spray coating the misted solution, or dip coating in a solution bath. Lastly, the wet film is dried [40]. If precursor solution and substrate wetting phases are succeeded, CSD represents a rapid and cost-effective method for synthesizing high quality electronic oxide thin films.

### 3.1.2 Spin coating

Spin coating is a procedure used to deposit films on a flat substrate. Usually a small amount of coating material applied on the center than substrate is accelerated to the desired speed so excess of liquid delivers to the surface of substrate to be coated and wetted it. Result of spinning at the constant rate fluid on the substrate starts to be thinner. Subsequently, the film drying stage begins [41].

### 3.1.3 Chemical vapor deposition

CVD involves flowing a precursor gas or gases into a chamber containing one or more heated objects to be coated. Chemical reactions occur on and near the hot surfaces, resulting in the deposition of a thin film on the surface [42].

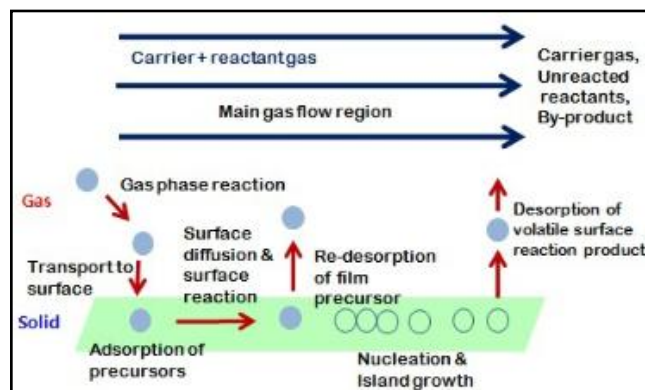


Figure 3.1 CVD mechanism [43]

## **3.2 Physical Deposition**

Physical deposition uses mechanical, electromechanical or thermodynamic means to produce a thin film of solid instead of chemical reactions. This technique is mostly known as physical vapor deposition. Sputtering and pulsed laser deposition techniques are used in this work so this section includes definitions and explanations about them.

### **3.2.1 Sputter processing**

Sputter deposition is basically defined as a process in which condensation of ejected atoms onto a sample to produce a thin film of these atoms. Ejected atoms are acquired from a target material by accelerated ionized atoms [44].

The sputtering process occurs in a vacuum chamber. The main components in the sputter chamber are target material, substrate, sputtering gas (an inert gas) and sputtering source. Target materials which are deposited on the substrates can be metal oxides (zinc oxide, titanium dioxide, tin oxide etc.), gold and silver. Sputtering gas is often argon. Sputtering source is used to accelerate the bombardment ion so it can be direct current (DC) or radio frequency (RF).

DC power supply is mostly used for conducting targets sputtering. In case of insulating or semiconducting targets, an RF power supply is required [45].

During sputtering process firstly, electrically neutral Argon atoms are introduced into a vacuum chamber at a pressure of 1 to 10 mTorr [45]. Between target and substrate a DC voltage is placed to ionize Argon atoms and create plasma. This plasma is also called a glow discharge because of its light emitting feature. At the same time, ionized Argon ions accelerated to the target for atom ejecting. Ejected atoms go through the substrate and deposit. Figure 3.2 shows a schematic illustration of sputtering process.

Addition a magnetic field to the basic DC sputtering system benefits to direct the ejected atoms to spiral magnetic flux lines near the target instead of being attracted toward the substrate. The main advantage of this is the plasma restricted to an area near the target, without causing damages to the thin film being formed.

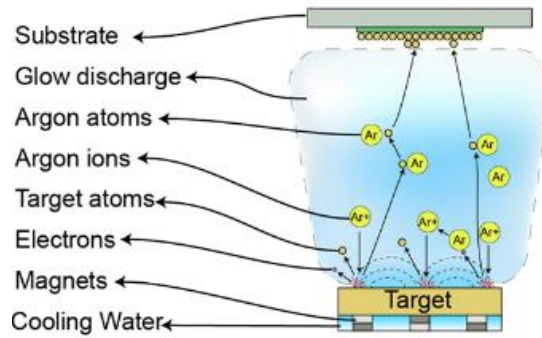


Figure 3.2 Schematic representation of sputtering process

The same type of physical process can also be done to remove unwanted material from a sample, in which case the ejected atoms can be collected on the chamber shielding. The process is called “sputter etching” [44]. Etching is selective removal of thin films result a desired thin film pattern. It is used micro fabrication with masks to protect the certain surface. Figure 3.3 shows the illustration of etching process.

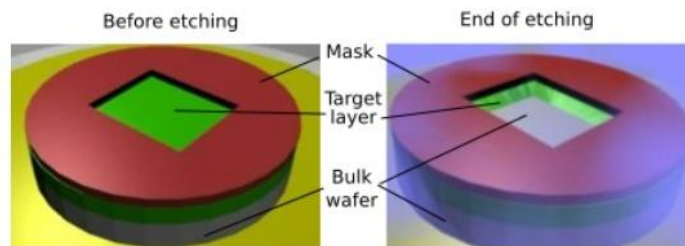


Figure 3.3 Etching illustration

### 3.2.2 Pulsed laser deposition

Pulsed laser deposition (PLD) is a deposition technique which is used to prepare thin films by ablation of one or more targets are illuminated by a focused pulsed- laser beam.

This technique was first used in 1960 after first experiments; it is used by Smith and Turner as a directed energy source for evaporative film growth in 1965. In late of 1980s PLD used for oxide film growth successfully. During years PLD development continued and it gained an important place for academic researches. Today in the deposition of insulators, semiconductors, metals, polymers and rarely biologic materials PLD technique is used [46]. It is mostly used small scale areas.

This process can be crudely split into two sections; first one is the plasma creation and expansion, second one is film growth at the substrate. First of all these steps occur in an ultrahigh vacuum chamber (UHV), elementary or alloy targets are stuck at an angle of  $45^\circ$  by a pulsed and focused laser beam. Substrates are placed with the surface parallel to the target surface at a target to substrate distance is typically 2-10 cm [47]. At the plasma creation section, high power laser pulses are used to melt, evaporate and ionize material from the surface of a target. This event is known “ablation” or “evaporation”. Ablation produces a transient, highly luminous plasma plume which extends away from the target surface. The plasma plume is defined as a vaporized material which includes neutrals, ions, and electrons. Ablation part is followed by film growth section. This occurs on a substrate by condensing the plume material and growing the thin film. The PLD set-up is shown on Figure 3.4.

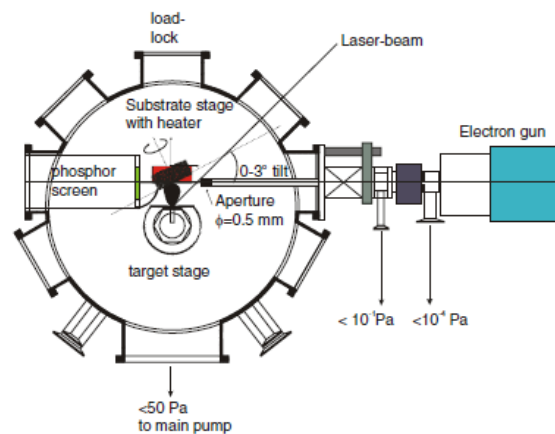


Figure 3.4 Schematic diagram of PLD set-up in University of Twente [48]

As it is mentioned above PLD is advanced method for small scale areas. Although there are many applications (nanoelectronics and photonics, energy, nanobiotechnology and nanomedicine) PLD could not answer large scale industrial needs because of its area controlled growth. But recentlyl arge area deposition is became available, able to grow thin films on wafers, up to 200 mm diameter (Figure 3.5) [48].



Figure 3.5 Scailing the synthesis of nanaomaterials: from 5x5 mm<sup>2</sup> to 200 mm wafer size [48]

- ***Pulsed laser deposition of TiO<sub>2</sub> and Cu<sub>x</sub>O in literature***

During PLD, many experimental parameters can be changed, which then have a strong influence on film properties. The laser parameters; laser fluence, wavelenght, pulse duration and repetition rate, the preperation conditions; target to substrate distance, substrate temperature, background gas and pressure are variable features for influence the film growth. Since pressure and temperature are mainly effective parameters on thin films, in this part of this work, will be mentioned about some research results about these properties.

The TiO<sub>2</sub> different crystal structures; anatase and rutile was observed under increasing oxygen partial pressure at fixed temperature by Syarif et al. (2002) [49]. TiO<sub>2</sub> films were deposited on glass substrates by PLD technique; with sintered TiO<sub>2</sub> pellet target, at 10 Hz repetation rate, at different oxygen partial pressure from 5 to 90 mTorr. The deposition time was fixed 90 min. Film thicknesses were determined range from 130 to 330 nm at 5-90 mTorr respectively. They obtained rutile crystal structure when oxygen partial pressure was 5 mTorr and anatase structure crystals when partial pressure 20-90 mTorr. The measured band gaps were 3.02 eV (5 mTorr) and 3.20 eV (20-90 mTorr).

Cui et al. (2012) deposited nanocrystalline TiO<sub>2</sub> films from metallic titanium at low temperatures by pulsed laser deposition with the assistance of  $4 \times 10^{-2}$  Pa oxygen plasma [50]. Single crystalline and transparent fused silica plates were used as the substrates. In the environment of pure oxygen plasma, metallic titanium target was ablated by focused laser pulsed. The as deposited films show a mixed anatase and rutile and exhibit good optical transparency in the visible and near infrared region.

Improvement of crystallinity was processed by annealing. Results after annealing at 900°C are shown complete transition to pure rutile nanocrystalline structure. They worked on three different annealing temperatures (300°C, 600°C and 900°C) to observe these changes. When the annealing temperature further increased the band gap energy shows a decreasing tendency. While as deposited film band gap value ( $E_g$ ) was determined 3.25 eV, after annealing at 300°C it is 3.30 eV, for 600°C and 900°C were 3.25 and 3.24 eV respectively.

Another article which is about the effect of oxygen partial pressure on PLD deposited  $TiO_2$  was recorded by Balakrishnan et al. (2013) [51]. They deposited nanocrystalline  $TiO_2$  thin films on silicon and quartz substrates at various oxygen partial pressures in range  $1 \times 10^{-5}$ - $3.5 \times 10^{-1}$  mbar with a substrate temperature 973 K. The studies indicated the formation of mixed phase at higher oxygen partial pressures and strong rutile phase at lower oxygen partial pressures. In addition, band gap values of thin films increased from 3.20 eV to 3.60 eV by increasing oxygen partial pressure.

As in  $TiO_2$  phase formation, oxygen pressure also influences copper oxide structural properties. Chen et al. (2008) studied different temperatures and pressures for copper oxide deposition by PLD [52].  $Cu_2O$  and  $CuO$  thin films grown on silicon substrates by using  $CuO$  target. Firstly, film growth performed at 500°C and under 0.004-32 Pa pressure range. Further increasing pressure ( $>0.04$  Pa) the  $CuO$  thin films are obtained. Afterwards, under 0.04 Pa pressure and at 400-700°C temperature range, thin films were deposited and further increasing substrate temperature  $CuO_2$  film modification was obtained. Besides, while oxygen partial pressure increased, 0.04-0.4-32 Pa, band gap values decreased, 2.52-2.42-2.12 eV, respectively.

### EXPERIMENTAL DETAILS

PV devices were based on a single p-n junction between as an n-type material,  $\text{TiO}_2$  and p-type material  $\text{Cu}_2\text{O}$ .  $\text{TiO}_2$  layer was deposited on a TCO, glass with FTO or ITO. For the back contacts gold were preferred.

FTO and ITO are mostly used as TCO substrates in photovoltaic devices. They are acting window layers for light to pass through the active layer where carrier generation occurs. Strong transparent and conductive surface are important properties to be used as a thin film electrode in a photovoltaic device.

$\text{TiO}_2$  is famous material with its diverse applications. It is most widely used in these applications; as white pigment with its brightness, UV blocker because of absorbing UV light and photo catalyst.  $\text{TiO}_2$  is known with its three crystal forms; anatase (tetragonal), rutile (tetragonal) and brookite (orthorhombic) (Figure 4.1). Rutile is the most stable form and anatase to rutile transition is possible at high temperatures. But anatase is well known with its excellent photocatalytic behavior and its 3.2 eV band gap is larger than rutile which is 3.0 eV. It is an n-type semiconductor with large indirect band gap and usually transparent in a wide spectral range between visible and infrared. Large band gap of a transparent film an important parameter to extract more power from sun. When  $\text{TiO}_2$  is located on the top side of the device; electron-holes pairs can only be performed by UV light on  $\text{TiO}_2$  so it will allow the photons to pass through the absorber layer which have less band gap energy. Besides, the excited electrons on the conduction band of  $\text{Cu}_2\text{O}$  would transfer to  $\text{TiO}_2$  while generated holes in valence band of  $\text{Cu}_2\text{O}$  prefer to opposite transfer and  $\text{TiO}_2/\text{Cu}_2\text{O}$  junction will



separate charge carriers effectively. Therefore, this TiO<sub>2</sub>/Cu<sub>2</sub>O p-n junction exhibits promising system for solar cells.

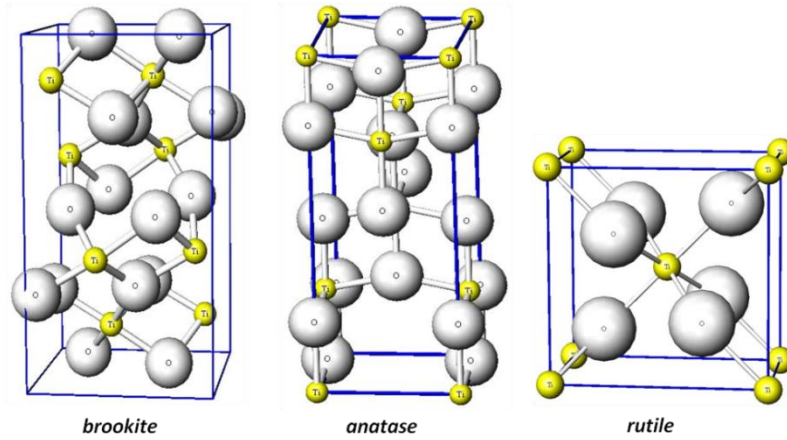


Figure 4.1 Crystal forms of TiO<sub>2</sub> [53]

Copper oxide, has three phases as it is seen at Figure 4.2; CuO (cupric oxide), Cu<sub>2</sub>O (cuprous oxide) and Cu<sub>4</sub>O<sub>3</sub> (paramelaconite) [54]. CuO and Cu<sub>2</sub>O are attractive materials for photovoltaic applications because of their abundance of raw material, cheap producing methods and favorable electrical properties. Both of them are p-type material with direct narrow band gaps. For Cu<sub>2</sub>O band gap is mostly known as 2.0 eV but this value depends on the fabrication methods so it can be represented between 2.0-2.6 eV and CuO it is 1.3-2.1 eV. If we compare these two phases maximum theoretical efficiencies according to Shockley-Queisser limit, Cu<sub>2</sub>O almost 23% and for CuO it is near 30% [2]. But at many researches the efficiency of CuO solar cell is quite low. The band gap of a semiconductor is not only parameter to estimate the efficiency, its carrier lifetime is also important. Cu<sub>2</sub>O has higher carrier lifetime than CuO [55] so it might be another reason to explain suitability of Cu<sub>2</sub>O as an active material for solar cells.

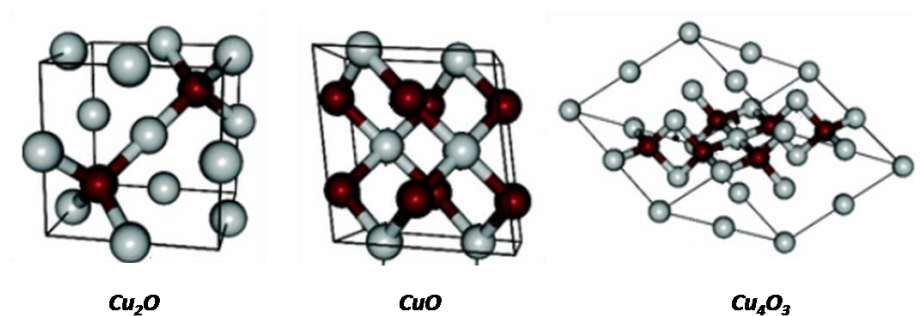


Figure 4.2 Crystal forms of copper oxide (gray:copper and red:oxygen atoms)[54]

Cu<sub>2</sub>O can absorb the photons which have larger energy than 2.0 eV. This energy equals to a photon's energy at 620 nm. In other words, Cu<sub>2</sub>O absorption range is between visible and ultraviolet sunlight range which involves 53% of sunlight.

Table 4.1 summarizes the roles of functional layers in thin film solar cell which was explained above. In this table, layer types express glass with FTO or ITO and TiO<sub>2</sub> together as substrate, FTO or ITO as front contact, Cu<sub>2</sub>O as absorber and gold as back contact.

Table 4.1 List the four types of layers in thin film solar cell together with their specific tasks and requirements necessary for an efficient solar cell[56]

<i>Layer type</i>	<i>Possible tasks and requirements</i>
Substrate	Mechanical and thermal stability, transparency
Front contact	Light trapping, antireflection, electrical contact, charge extraction, transparency
Absorber	Absorb light, charge extraction, low recombination
Back contact	Electrical contact, charge extraction

To understand the following experimental part's proceeding way, repetition of aims in that work will be useful. First aim is to achieve the anatase crystalline TiO<sub>2</sub> phase growing on the substrates. This part was completed by using commercial FTO substrates. Afterwards, to enhance the crystallinity of TiO<sub>2</sub> another substrate ITO was used. Second aim is to achieve Cu<sub>2</sub>O growing on the TiO<sub>2</sub> layer. Cu<sub>2</sub>O growing experiments were completed on the TiO<sub>2</sub> layers which were provided from project collaborator in Israel Bar Ilan University, since these samples had pure anatase phase. After determination of optimum deposition conditions for both TiO<sub>2</sub> and Cu<sub>2</sub>O layers, photovoltaic cells were produced on these conditions and gold was used for the back contact. Gold layer was prepared by sputtering method.

#### **4.1 p-n Heterojunction Photovoltaic Cell Process Conditions**

In this part, samples' electron conductor layer as a p-side; TiO<sub>2</sub> deposition and active layer as an n-side; Cu<sub>2</sub>O deposition conditions will be explained.

#### 4.1.1 Sample preparation for deposition

Commercial substrates both FTO and ITO were used. FTO substrates specifications: 6.7x6.7 mm<sup>2</sup> size and a sheet resistance of 15  $\Omega$  per square (TEC 15, Hatford Glass Co. Inc.). ITO substrate specifications: approximately of 9x9 mm<sup>2</sup> size and  $3 \times 10^{-4}$   $\Omega$  per cm resistance (SolMateS B.V). They were cleaned properly before deposition by using acetone and ethyl alcohol. First of all they were kept in acetone 5 minutes in ultrasonic bath. After that they were washed by ethyl alcohol and dried under nitrogen stream. Following this cleaning part all samples were viewed under microscope and if there were some surface dirtiness, cleaning part was repeated.

#### 4.1.2 TiO<sub>2</sub> deposition on FTO substrate

TiO<sub>2</sub> layer was deposited by pulsed laser deposition (Figure 4.3) consisting of a KrF excimer laser with 248 nm wavelength (Coherent). Laser was operated at the repetition rate of 8 Hz. The laser was directed to target, as explained at Chapter 3 pulsed laser deposition part, for plasma plume creation. Two different targets were used. One of them has been prepared from commercially available TiO<sub>2</sub> powder by sinterization. This target was called at following steps "TiO<sub>2</sub>-powder target". Another target was pure single crystal anatase which was called "TiO<sub>2</sub>-crystalline target". During deposition target was moved right to left to prevent the target surface drilling. Because of using very small area substrates, substrate rotation wasn't necessary to produce homogenous films. Substrate was attached sample stage by using silver paste then sample stage was placed to sample holder which is mounted to a heater in the PLD chamber. Target to substrate distance was 5 cm.

TiO<sub>2</sub> deposition was carried out on FTO substrates at 0.4 mbar oxygen pressure, variable temperatures from 350°C to 550°C and during 60 minutes deposition time. Samples were called FTO350, FTO450 and FTO550 related with their deposition temperatures, respectively. During deposition of these samples TiO<sub>2</sub>-powder target was used.

After deposition, structural and optical measurements have been done. Because of achieving amorphous to crystalline transformation, samples were annealed at 600°C. Annealed samples' structural and optical measurements have done, too.

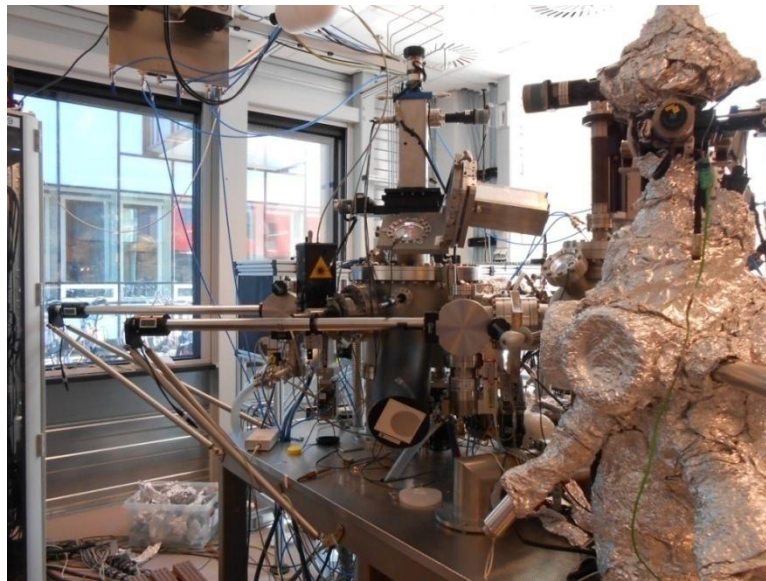


Figure 4.3 Pulsed Laser Deposition in University of Twente

#### 4.1.3 Sample cleaning after deposition

After deposition, glass side of the samples which stacked to sample stage by silver paste had yellowish appearance. Acetone and ethyl alcohol chemicals weren't successful remover to clean this stain. The stain looks inside the glass layer of the substrates. With taking account silver can be used to prepare silver nanoparticle glass under high temperatures [57], all samples' absorbance measurements were done. They showed a sharp peak around 400 nm. According to reference [57] UV-Visible absorption spectra showed strong absorption band centered at 410 nm and the absorbance increased as a function of silver content. Besides, glass color was changing from opaque to yellow-brownish with increasing silver content. The appearances of some samples in the present experiment and absorbance spectra can be seen on Figure 4.4. Considering with this figure we can say that during the deposition silver paste insert the glass and it causes the yellow stains.

To overcome this problem, grinding papers with 30  $\mu\text{m}$  and 10  $\mu\text{m}$  grain size (Struers SiC Foil) were used respectively. After these grinding and polishing part, absorbance measurements were repeated and it was seen that the peak around 410 nm was

disappeared. FTO14 was the heavily yellowish sample so its before and after grinding absorbance spectra is illustrated on Figure 4.5.

After grinding and polishing, samples kept in acetone for 5 minutes then washed with ethyl alcohol.

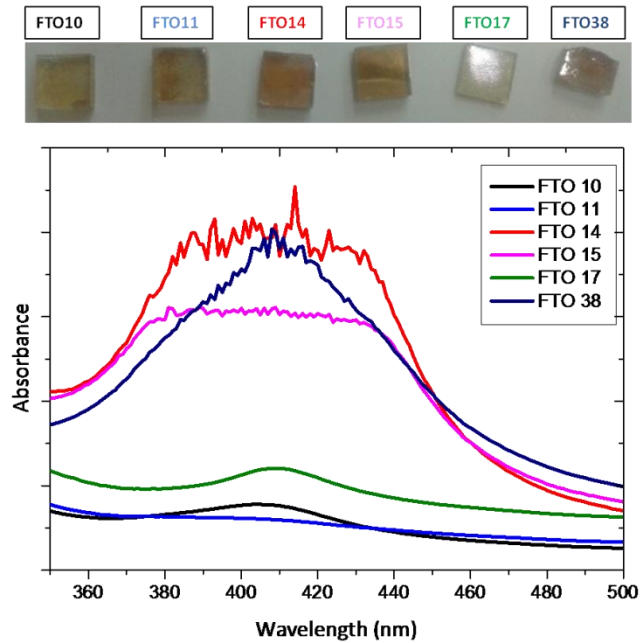


Figure 4.4 Absorbance spectra of yellowish-glass substrates

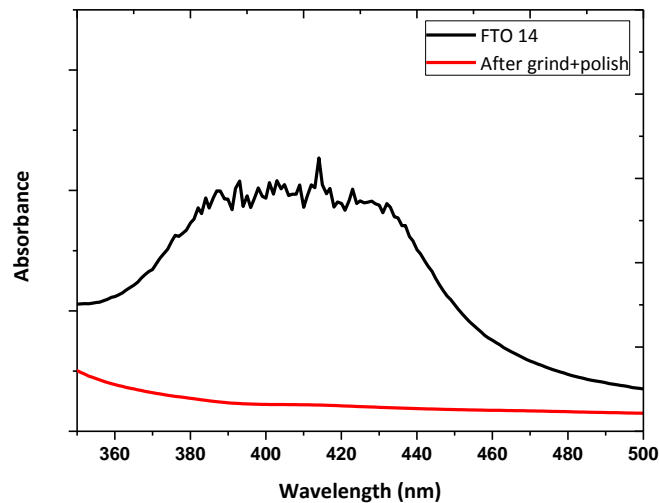


Figure 4.5 Absorbance spectra of yellowish glass substrate before and after grinding

#### **4.1.4 TiO<sub>2</sub> deposition on ITO substrate**

Pulsed laser deposition was carried on ITO substrates at 500°C and two different pressures; 0.05 mbar and 0.2 mbar. The samples were called ITO005 and ITO02 related with their deposition pressures, respectively. TiO<sub>2</sub>-crystalline target was used. Other deposition parameters were same as 4.1.2. After deposition cleaning step was also done as 4.1.3.

Inspection of samples at different conditions and with different substrates were directed the experiments through photovoltaic cell's junction's n type side. Next step was determining to growth parameters for p type side: Cu<sub>2</sub>O which will be explained at following part.

#### **4.1.5 Active layer deposition**

Copper oxide deposition experiments were done on the pure anatase grown FTO substrates which were provided from Bar Ilan University. PLD was set-up as reference [39] but different from this reference target material was CuO instead of Cu<sub>2</sub>O.

Copper oxide layer deposition was performed at 400°C and under 0.2 mbar total pressure in the chamber together with argon and oxygen. Oxygen partial pressure was regulated to achieve Cu<sub>2</sub>O crystal phase. Three different pressures was used; without oxygen (only 0.2 mbar Ar atmosphere),  $2 \times 10^{-4}$  mbar and  $2 \times 10^{-2}$  mbar oxygen partial pressures. The effect of variable oxygen pressures on Cu<sub>2</sub>O and CuO phase growth was observed by XRD. Different Cu<sub>x</sub>O composition's absorbance spectra were measured by spectrophotometer and band gap values were estimated by Tauc plot.

#### **4.1.6 Overall photovoltaic cell deposition**

After deposition parameters of individual layers were defined, overall photovoltaic cell was produced on ITO substrate. TiO<sub>2</sub> deposition was carried on 0.08 mbar oxygen pressure and 500°C temperature. Cu<sub>2</sub>O deposition was proceeding under 0.2 mbar total pressure of argon and oxygen. Oxygen partial pressure was  $2 \times 10^{-4}$  mbar and temperature was 400°C.

To make two electrode shapes onto solar cell, ITO substrate's 2-3 mm part was covered before deposition. Thus, covered part wasn't deposited to use ITO one of the contacts and without covering part was deposited with  $\text{TiO}_2$  and  $\text{Cu}_2\text{O}$  respectively (Figure 4.6).

#### **4.1.7 Bottom layer deposition (back contact)**

Good electrical contacts are very important parameters to make electrical characterization of cell accurately. To provide an electrical contact, substrate, ITO was used as one of the electrodes and it was covered with gold layer to make it better contact. For another electrode, gold was sputtered on the  $\text{Cu}_2\text{O}$  layer.

Gold contacts were deposited by radio frequency sputtering method from gold target and using argon as a sputtering gas. Perkin Elmer RF Sputtering System 2400 was used at 0.02 mbar argon pressure, 6 minutes (about 240 nm). To provide steady gold bonding, both copper and ITO parts were etched for 1 min (equals to 2 nm) before deposition.

During the sputtering, 0.2 nm thick copper sheets were used as homemade masks. Every mask had one large hole with vary diameters from 2.9 to 4 mm for onto  $\text{Cu}_2\text{O}$  patche and one small hole with vary diameters from 1 to 2 mm. These dimensions were aligned corresponding with overall solar cell surface shape.

Overview of overall photovoltaic cell layers before-after PLD and before-after sputtering can be seen on Figure 4.6.

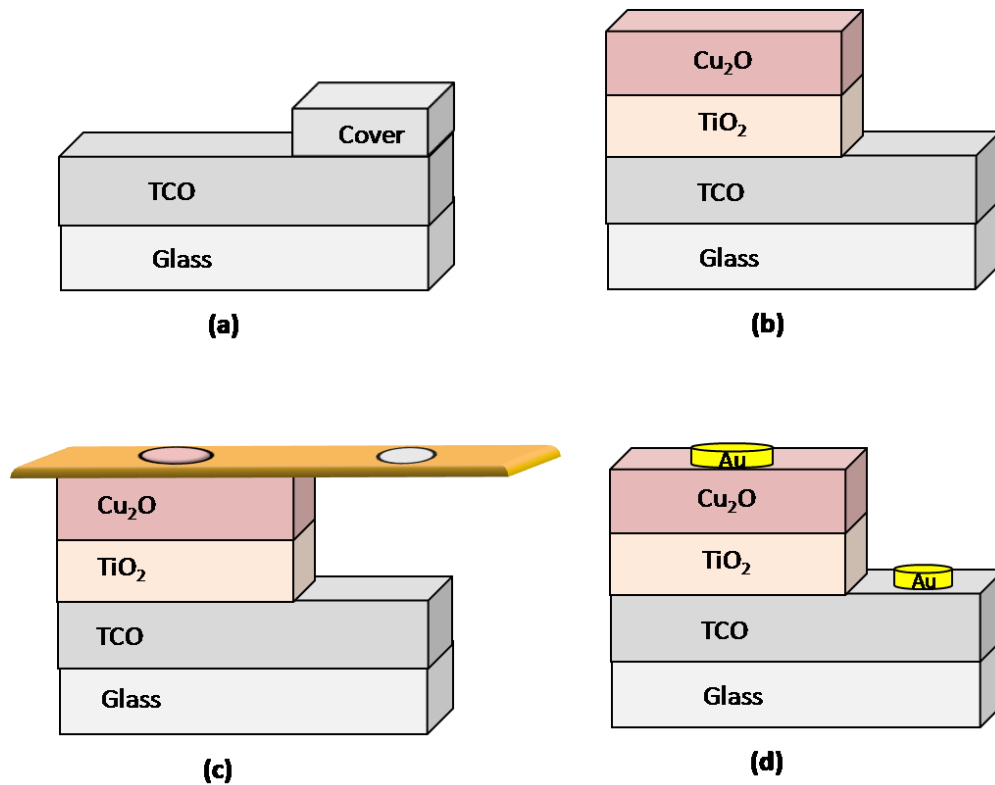


Figure 4.6 Overview of overall photovoltaic cell layers (a) with covered part before PLD (b) after PLD (c) before gold sputtering with mask (d) after gold sputtering (TCO: ITO or FTO)

## 4.2 Sample Inspection and Characterization

Crystal structures of samples were investigated by XRD (PANalytical X'Pert Pro). Optical measurements; transmittance and absorbance spectra of films were completed by using spectrophotometer (VARIAN CARY 50 Scan UV-Visible Spectrophotometer) in the wavelength range from 200-1000 nm. To investigate the film thickness, cross sectional views were presented by scanning electron microscopy (Zeiss MERLIN HR-SEM).

### 4.2.1 Illumination set-up

An illumination set-up was arranged to investigate the electrical properties of solar cells. Figure 4.7 shows the components of this set-up and Table 4.2 includes properties of the components. A photo conductance tool which is suitable for analysis of carrier recombination lifetime was tested with a commercially available silicon solar cell (MC-SP0.8-NF-GCS) to make it operational for obtaining I-V curves of photovoltaic cells which were produced in this study.



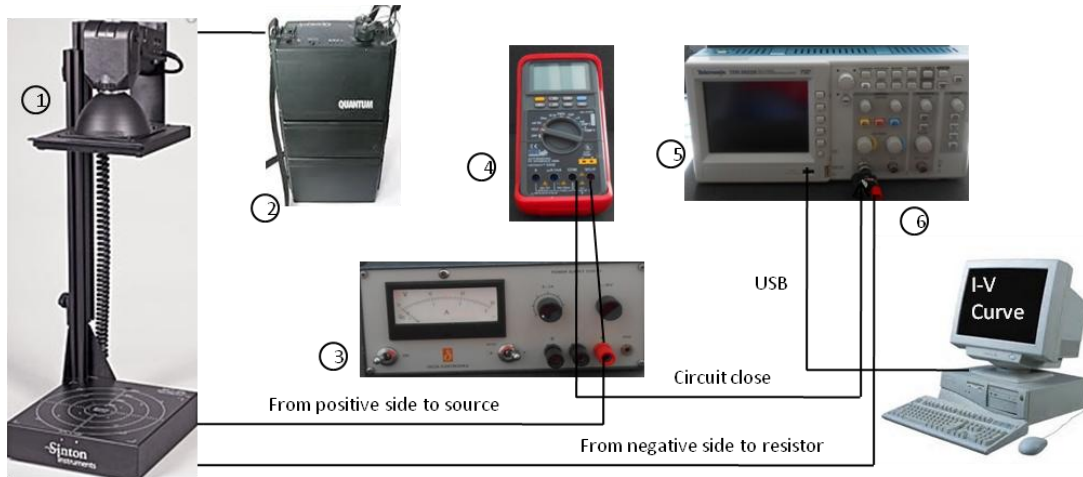


Figure 4.7 Illumination set-up

Table 4.2 Illumination set-up components

Label	Component Name
1	WCT-100 Photoductance Tool, SINTON Consulting Inc.
2	Quantum Qpaq Model X Battery
3	Delta Elektronika Power Supply E030-3
4	Voltcraft 350E Multimeter
5	Tektronix TDS 2022B-Two Channel Digital Storage Oscilloscope
6	Resistor

Photo conductance tool's flash head was operated under 400W.s and 1 sun conditions and during the measurements it was connected to battery. Solar cell was put on the sample stage and it was connected to source and resistor as related with the forwarding bias, as it is seen at Figure 4.8.

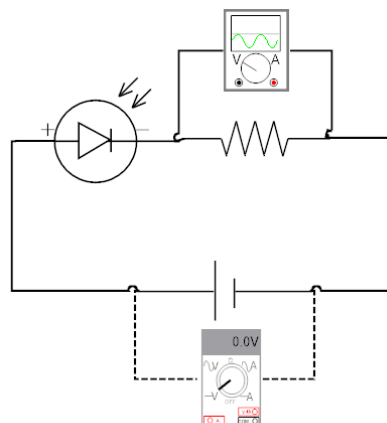


Figure 4.8 Circuit elements connection

Lamp holder is suitable to switch light to sample distance and this distance was very effective on the light intensity. In addition, lamp has two type of light; one of them is continuous light and short flash. Short flash is suitable for long lifetime material ( $>100 \mu\text{s}$ ). Assuming that thin film PVs lifetime will be lower than this, experiments were carried on continuous light.

First experiments were done with different resistors from 18.5 ohm to 831 ohm. Measurements have been taken under 27 cm continuous light distances and between 0-4 voltages with 0.1 V steps. As it is seen at Figure 4.9 while external resistor in the circuit is increased, I-V curve shows tendency to be linear. To determine  $P_{\text{max}}$  and FF values from this curve, it should be similar Figure 2.10 so 46.6 ohm resistor was used in the electrical circuit. These results show that  $I_{\text{sc}}$  is  $3.1 \times 10^{-3}$  A and  $V_{\text{oc}}$  is 3.25 V in this circuit. Silicon solar cell (SP08) has been provided from a company with its data sheet which includes all  $I_{\text{sc}}$ ,  $V_{\text{oc}}$ ,  $I_{\text{max}}$  and  $V_{\text{max}}$ . According to certified specifications;  $I_{\text{sc}}$  is 0.23 A and  $V_{\text{oc}}$  is 4.80 V. But in the present set-up, these values were lower than them. This might be because of the low light intensity. Therefore, all measurements were repeated after light to sample distance was regulated as 5 cm to increase light irradiance on the cell.

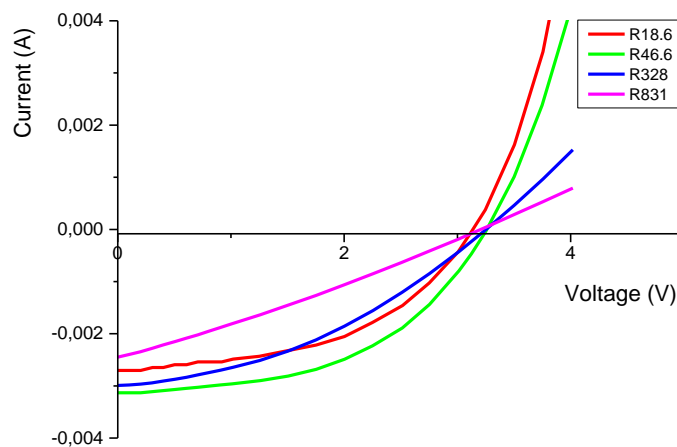


Figure 4.9 Resistor effect on I-V curve

Figure 4.10 shows the current-voltage data which were taken when the light length was 5 cm from the SP08. Only forwarding bias results were illustrated and curve shifted up side to make the results more obvious. As it is seen on the figure,  $I_{\text{sc}}=1.1 \times 10^{-2}$  A,  $V_{\text{oc}}=4.16$  V,  $I_{\text{max}}=0.9 \times 10^{-2}$  and  $V_{\text{max}}=3.24$  V. Related with these results, fill

factor was calculated; 0.63. These results were also lower than solar cell's specifications. Certified current voltage characteristic of SP08 was given at Figure 4.11.

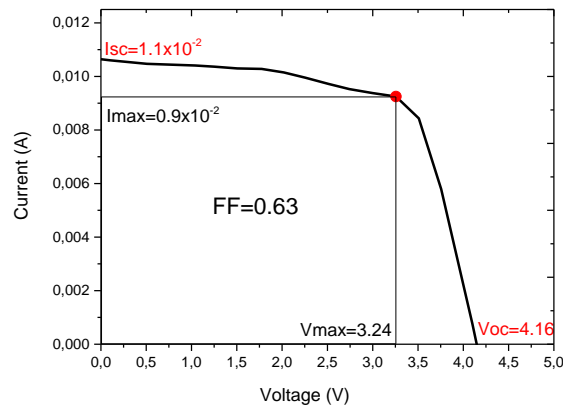


Figure 4.10 I-V curve of SP08 at illumination set-up

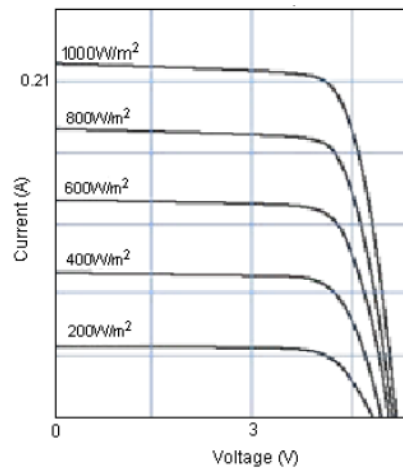


Figure 4.11 I-V curve of SP08 at various irradiance levels

Table 4.3 shows difference between current-voltage characteristic results of SP08 under  $1000\text{W/m}^2$  irradiance and measurement results at homemade illumination set-up.

Table 4.3 Comparison of silicon solar cell certified specifications and solar simulator set-up

(Area of module= $0.014\text{ m}^2$ )	<b>Certified specifications</b>	<b>Illumination set-up</b>
Open circuit voltage ( $V_{oc}$ )	4.80 V	4.16 V
Short circuit current ( $I_{sc}$ )	0.23 A	$1.1 \times 10^{-2}$ A
Maximum power voltage ( $V_{max}$ )	3.85 V	3.24 V
Maximum power current ( $I_{max}$ )	0.21 A	$0.9 \times 10^{-2}$ A
Fill factor (FF)	0.73	0.65

Assuming that solar cell's power efficiency should be same on different measurement techniques, homemade illumination set-up irradiance might be estimated. SP08's power efficiency was calculated by using equation (2.7) with Table 4.3.

Power efficiency of SP08;

$$\eta = \frac{(4.80) \times (0.23) \times (0.73)}{(0.014) \times 1000} \quad \eta = 0.058 \text{ (\%5.8)}$$

If this efficiency is equalized to illumination set-up results;

$$0.058 = \frac{(4.16) \times (1.1 \times 10^{-2}) \times (0.65)}{(0.014) \times P} \quad P = 37 \text{ W/m}^2$$

Illumination set-up irradiance is estimated  $37 \text{ W/m}^2$  which is lower than the lowest irradiance level at the Figure 4.11. Considering that at lowest irradiance level  $I_{\max}$  is  $0.042 \text{ A}$ , in the present case  $0.9 \times 10^{-2} \text{ A}$   $I_{\max}$  might be acceptable for the  $37 \text{ W/m}^2$ .

To operate this set-up for thin filmsolar cells, it was necessary to make a suitable sample stage. Because their contacts at the back side and to probe these contacts, there should be a large space between PV and ground place. To overcome this, a simple sample stage was developed. Two copper lines were used for probing. But it was still problem to clamp source probes to these copper lines so two wires were soldered to these copper lines and probes were clamped them.

Figure 4.12 shows sample stage for thin film PVs and Figure 4.13 illustrates the position of thin film PV under illumination.



Figure 4.12 Sample stage for thin film PVs, (left) front and (right) behind

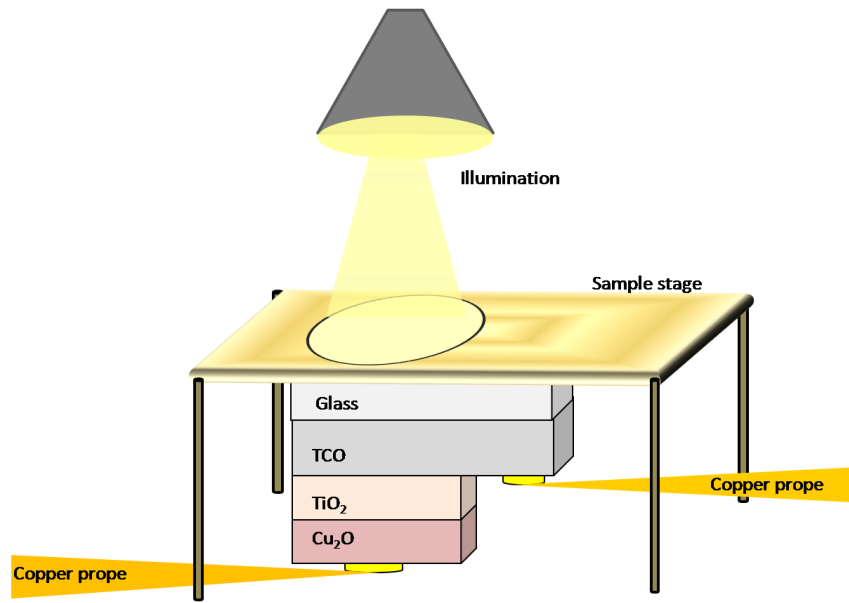


Figure 4.13 Illustration of thin film photovoltaic cell under illumination

### RESULTS AND DISCUSSION

In this chapter, experiment results were presented with the same topic order in Chapter 4. This chapter involves the discussion of experiment results of individual layers of photovoltaic cell and also overall cell characterization.

#### 5.1 TiO<sub>2</sub> Deposition Conditions

##### 5.1.1 TiO<sub>2</sub> deposition on FTO substrate

- *Film structure and morphology*

The controlled processing is important to achieve suitable properties on materials. As it is mentioned above, suitable property for TiO<sub>2</sub>, in this study, is anatase phase. Besides other deposition parameters, substrate temperature and oxygen pressure play important role to achieve high quality films using PLD. For this reason, considering that rutile phase grows at low pressures easily and anatase phase forms at higher oxygen pressures, at 0.4 mbar oxygen pressure, three different samples were produced. Deposition temperatures were 350°C, 450°C and 550°C. The TiO<sub>2</sub>-powder target was used. Under these conditions, according to the XRD results no either anatase or rutile peaks being formed. Films were subjected to thermal treatment at 600°C and only one of them which deposited under 350°C exhibited a weak anatase peak. This incipient crystalline might have been strong after second annealing so this film was annealed at 650°C. But XRD patterns showed that rutile peaks were formed. The XRD results were presented in Figure 5.1. After first annealing, film has anatase phase. After second annealing in addition to this anatase peak, two rutile peaks were formed. This formation can be explained with the anatase to rutile transformation at 600°C annealing temperature [58].

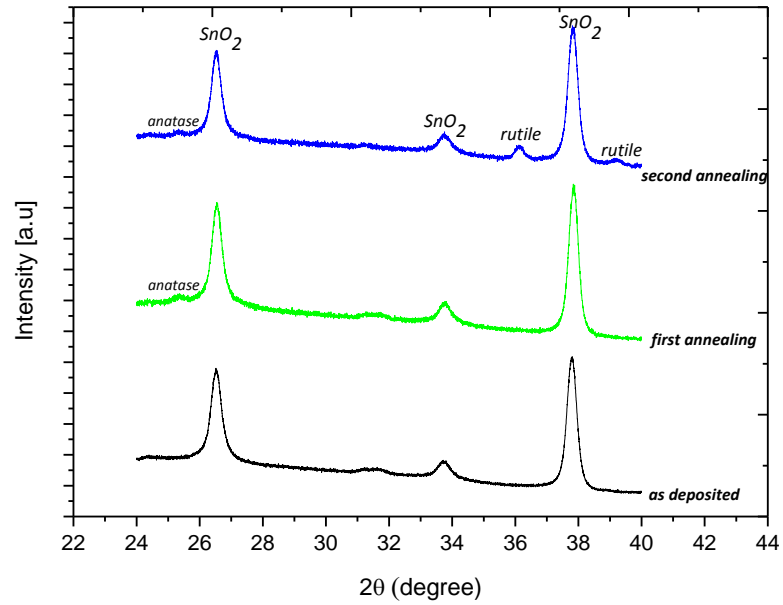


Figure 5.1 XRD patterns of FTO350 films

Following inspection was SEM analysis on surface morphology and the film cross section. Figure 5.2 shows that SEM image of FTO350 after annealing at  $650^\circ\text{C}$ . From cross section of film, first layer was approximately 250 nm thick FTO and top layer approximately 166 nm thick  $\text{TiO}_2$  film. It illustrates that film was compact on the cross section.

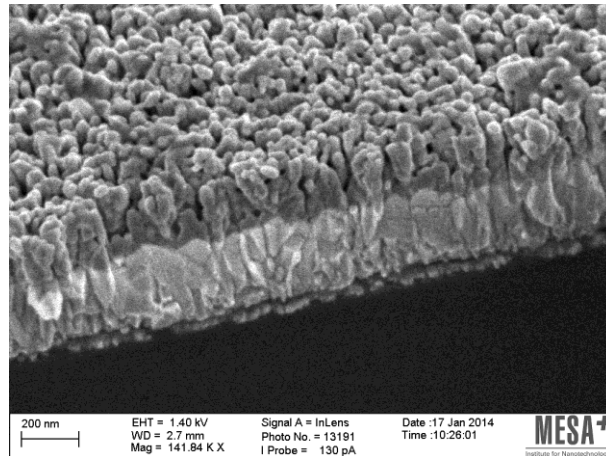


Figure 5.2 SEM image of  $\text{TiO}_2$  film deposited on FTO at  $350^\circ\text{C}$ , 0.4 mbar oxygen pressure, with  $\text{TiO}_2$  powder target

- **Optical properties**

Transmittance spectra was compared for two type of experiments; (i) for the samples which were deposited at 0.4 mbar and different deposition temperatures, (ii) FTO350 which was annealed at two different temperatures after deposition.

Figure 5.3 illustrates the optical transmission spectra of FTO350, FTO450 and FTO550 films. The red line on the graph shows that FTO substrate's transparency which is approximately 70% in near infrared and visible light ranges. It can be seen that the films exhibits a fall in transmittance at about 400 nm or 300 nm related with the film band gap of deposited TiO<sub>2</sub> films that starts absorbing UV light. The low temperature growth films exhibit high transparency in the visible and near infrared region.

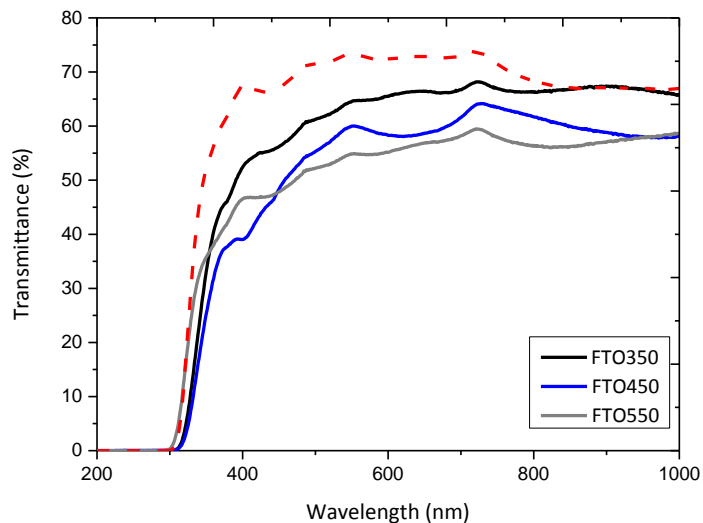


Figure 5.3 Optical transmission spectra of TiO<sub>2</sub> films deposited on FTO substrates

Figure 5.4 illustrates the optical transmission spectra of FTO350 as deposited, annealed at 600°C and annealed at 650°C films. It is clear that after annealing, transparency decreases comparison with the as deposited film. Considering that after annealing at 600°C film structure is anatase and after second annealing at 650°C film structure is anatase+rutile, first time annealed samples transparency range is larger than the other sample.

Figure 5.3 and Figure 5.4 illustrate that film transparency fall down whether annealing temperature increase or deposition temperature increase.



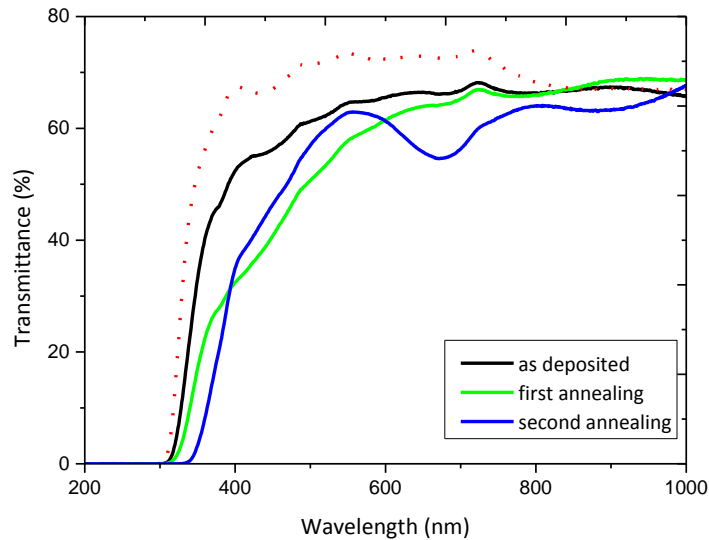


Figure 5.4 Optical transmission spectra of FTO350 as-deposited and annealed films

The transmission data was used to calculate indirect band gap ( $E_g$ ) of the films. Tauc plot parameters were calculated by using equations (2.1), (2.2) and (2.3). The values obtained from these data are shown in the Figure 5.5. As-deposited film's band gap was 3.45 eV. This value is only important as a starting point to observe the band gap changing with the structural transformation. Because the energy values generally depend on the film crystal structure. After annealing at 600°C film was anatase with 3.29 eV band gap. After annealing at 650°C, film was multicrystalline which shows anatase and rutile peaks together in XRD. Its band gap was 3.15 eV. These band gap values are comparable but little bit higher than the literature which mostly express anatase and rutile indirect band gap 3.20 eV and 3.0 eV respectively [10], [59]. Generally anatase phase has higher band gap than rutile phase. Comparison for present results with this general values; the band gap difference for the anatase film might be due to the poor crystallinity. For the multicrystalline film case, its band gap is also expected to be higher than pure rutile film's band gap which is 3.0 eV so 3.15 eV is possible. Furthermore, Figure 5.5 presents that the band gap energy shows decreasing tendency depending on the annealing temperature.

Table 5.1 shows different band gaps for different crystalline structure of FTO350.

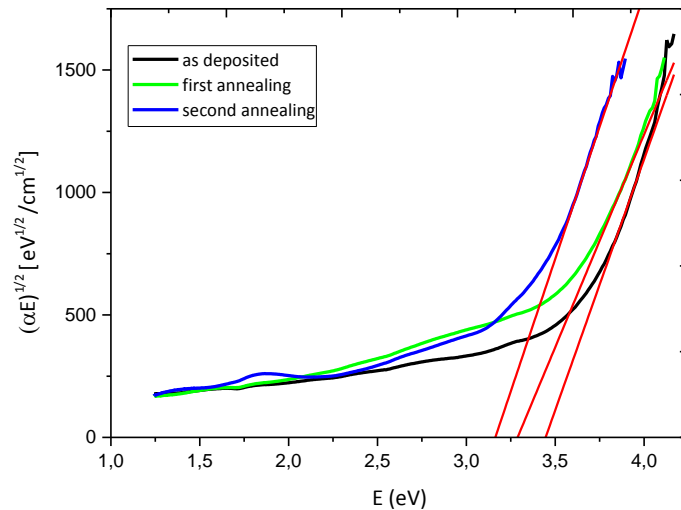


Figure 5.5 Optical indirect band gap data of FTO350 as-deposited and annealed films

Table 5.1 Sample structure and band gap of FTO350

<b>Sample name</b>	<b>Structure</b>	<b>Band gap (eV)</b>
FTO350as deposited	amorphous	3.45
FTO350 first annealing	anatase	3.29
FTO350 second annealing	anatase+rutile	3.15

Under same temperature and pressure deposition conditions as FTO350 another sample was produced by TiO<sub>2</sub>-crystalline target. According to XRD results, as-deposited film was amorphous. Thus, it is clarified that as-deposited film structure wasn't affected TiO<sub>2</sub> target is whether powder or single crystal anatase.

### 5.1.2 TiO<sub>2</sub> deposition on ITO substrate

- **Film structure and morphology**

TiO<sub>2</sub> growing on FTO substrates, under 0.4 mbar oxygen pressure and at 350°C temperature, it was amorphous phase but after annealing at 600°C it transformed to anatase phase. Therefore deposition carried out at 500°C and different pressures: 0.05 mbar and 0.2 mbar on the ITO substrates. Films were deposited from TiO<sub>2</sub>-crystalline target during 60 minutes.

XRD patterns of these films were illustrated at Figure 5.6 and Figure 5.7. Both of films showed crystalline after deposition. ITO005 has mixed anatase and rutile structure.

ITO02, anatase was the only one was detected. Although crystallinity was achieved, samples were annealed at 600°C but XRD patterns didn't change. Achieving the crystalline phase on as-deposited films makes preferable the ITO substrates as far as FTO substrates.

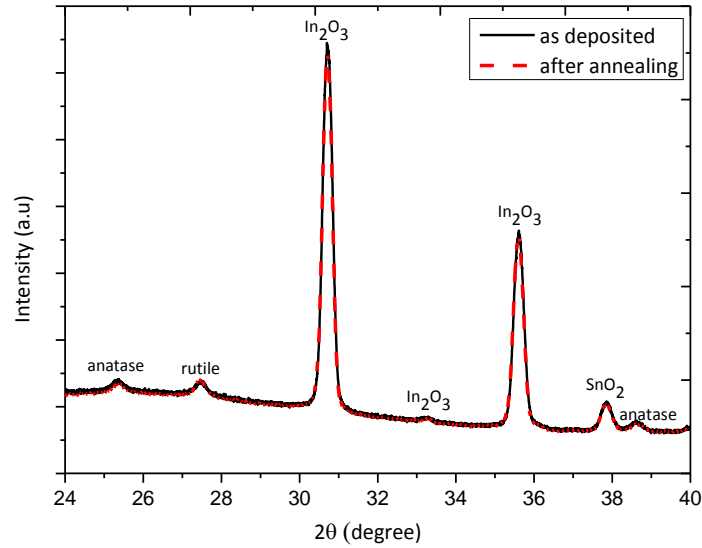


Figure 5.6 XRD of ITO005

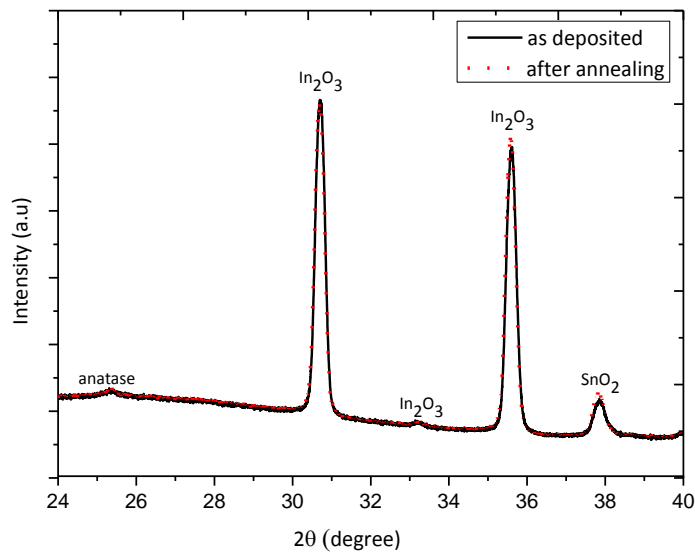


Figure 5.7 XRD of ITO02

Figure 5.8 presents SEM images of TiO<sub>2</sub> film growth on ITO substrates (a) ITO005 and (b) ITO02. At images first layer 195 nm ITO and second layer for ITO005 140 nm TiO<sub>2</sub>,

for ITO02 95 nm  $\text{TiO}_2$ . It is clear to observe that film cross sectional view is compact and surface is smooth.

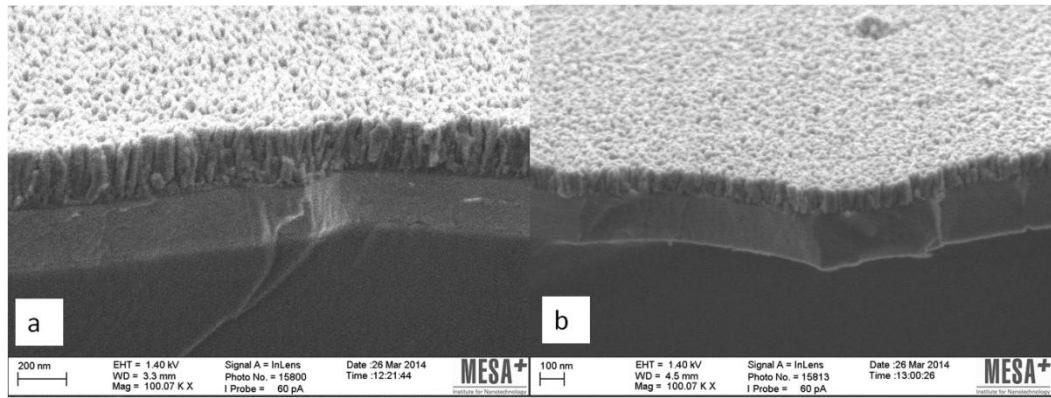


Figure 5.8 SEM images of  $\text{TiO}_2$  films deposited on ITO (a) 0.05 mbar (b) 0.2 mbar oxygen pressure

As a comparison of FTO and ITO substrates; for  $\text{TiO}_2$  growth in terms of the crystal structure, it is possible to get crystalline films on ITO without thermal treatment. This might be because of the ITO crystal structure is more convenient than the FTO structure to  $\text{TiO}_2$  crystal growth.

- **Optical properties**

Optical transmission spectra of ITO substrate based films were illustrated at Figure 5.9. Because of the flat surface of ITO substrate transmission spectra is wavelike. ITO substrates transparency approximately 65% between visible and infrared light range. After deposition, at 0.05 mbar oxygen pressure transparency was about 70% and at 0.2 mbar, it is 66%. This transmission difference might be explained with more porous structure after deposition in comparison with ITO substrate surface. According to reference [60] at lower gas pressures the film consists dense structure and at higher gas pressures columnar crystals with voids are deposited so at lower pressures films are compact and at higher pressure films are porous. When the film is porous light can pass through the voids and this will increase the transmittance. In other words, when oxygen pressure increases transmittance also increases because of the porous surface. On the other hand, it can be seen at Figure 5.9, different crystal structure and thickness are also effective on the transmittance. ITO005 thicker than ITO02 and its transparency lower.

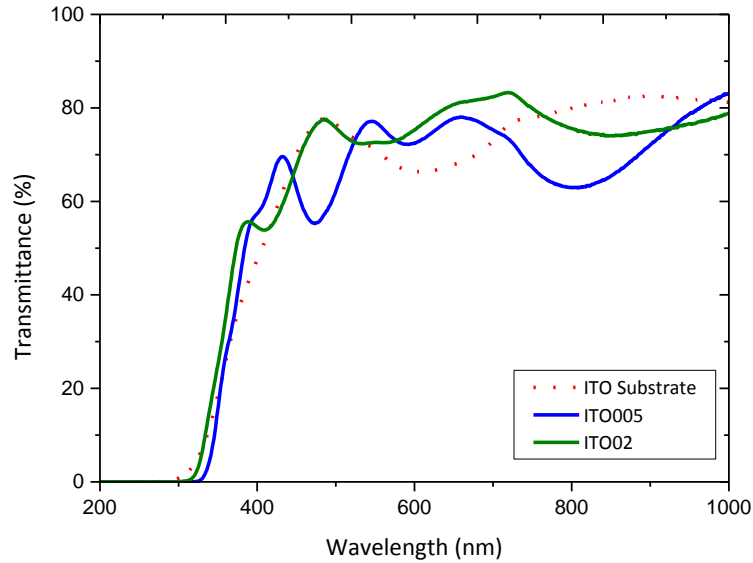


Figure 5.9 Optical transmission spectra of ITO005 and ITO02 as-deposited films

Transmission spectra were used to calculate band gap of films. Figure 5.10 shows that ITO005 film's indirect band gap 3.28 eV and ITO02 film's indirect band gap 3.33 eV. According to XRD patterns ITO02 has only anatase phase and ITO005 has anatase and rutile phase together. Band gap values are related with these phases, too. Anatase phase band gap is generally larger than rutile phase, as it is seen at this figure. These results are also comparable with the band gap of FTO based films in heading 5.1.1. Table 5.1 shows that anatase film on FTO has 3.29 eV band gap which is 3.33 eV for anatase film on ITO. Table 5.2 shows that anatase and rutile mixed phase on ITO has 3.28 eV band gap which is 3.15 eV for mixed phase on FTO. This difference might be because of anatase peaks more than rutile peaks on ITO substrates, so band gap is near the anatase's.

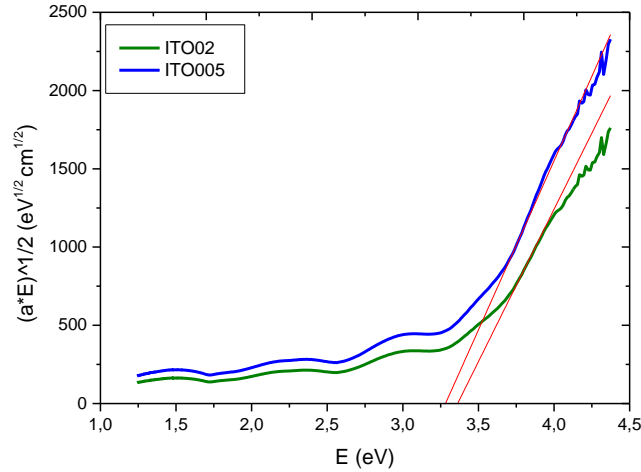


Figure 5.10 Optical indirect band gap data of ITO005 and ITO02 films

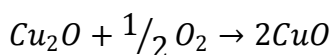
Table 5.2 Sample structure and band gap of ITO samples

<i>Sample name</i>	<i>Structure</i>	<i>Band gap (eV)</i>
ITO005	Anatase+rutile	3.28
ITO02	Anatase	3.33

### 5.1.3 Active layer deposition

- **Film structure and morphology**

As it was mentioned before, copper oxide deposition experiments were processed on TiO<sub>2</sub> deposited FTO substrates which were provided from a collaborator at Bar Ilan University. Figure 5.11 shows that XRD patterns of copper oxide films. It can be seen that Cu<sub>2</sub>O peaks decrease with the increasing oxygen pressure. When the oxygen pressure is 2x10<sup>-2</sup> mbar, Cu<sub>2</sub>O peaks at (111) and (200) planes disappears. Instead of these peaks (-111) plane CuO peak appears. While CuO indicates better crystallinity under high oxygen pressures, it is vice versa for Cu<sub>2</sub>O films. This might be explained with the following reaction:



With the increasing partial oxygen pressure Cu<sub>2</sub>O starts reacting with oxygen and CuO phase can be formed. Without oxygen case, argon pressure was 0.2 mbar during the deposition. Since argon is an inert gas, it doesn't react with copper. XRD patterns were

similar both without oxygen and  $2 \times 10^{-4}$  mbar oxygen partial pressure samples, except Cu peak at the without oxygen pattern. Due to the copper rich phases are limitation for solar cells [39],  $2 \times 10^{-4}$  mbar oxygen partial pressure is favorable to get  $\text{Cu}_2\text{O}$  phase.

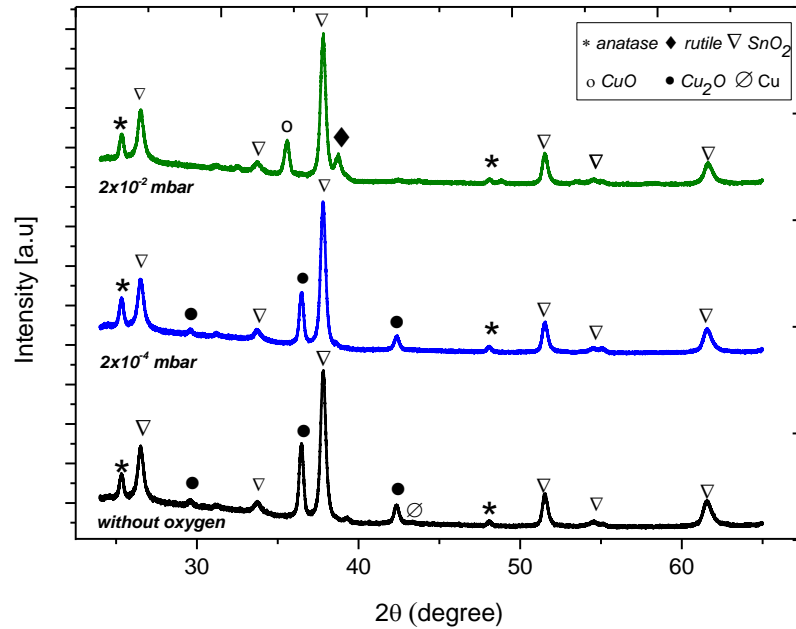


Figure 5.11 XRD patterns of copper oxide films prepared at 400°C and different oxygen partial pressures

Figure 5.12 shows SEM image of copper oxide layer which was deposited under  $2 \times 10^{-4}$  mbar oxygen partial pressure on  $\text{TiO}_2$  deposited FTO substrate. Thickness of copper oxide layer from cross section view is approximately 142 nm. It is clear to see that tetragonal structure of  $\text{TiO}_2$  and cubic structure of  $\text{Cu}_2\text{O}$ .

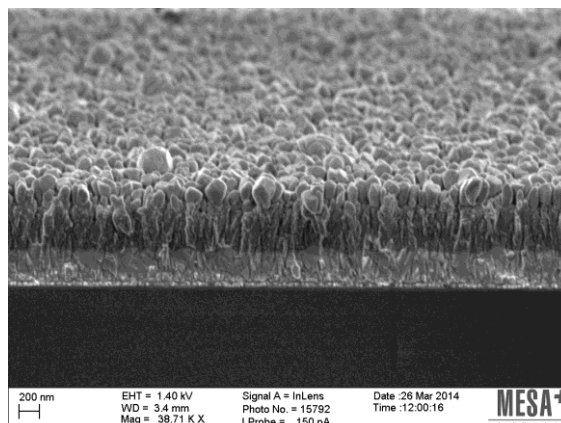


Figure 5.12 SEM image of copper oxide layer on  $\text{TiO}_2$  deposited FTO substrate

- **Optical properties**

Copper oxide layer is the active layer of photovoltaic cells so it is expected that it acts as an absorber under sunlight. Therefore absorbance spectra of copper oxide films were illustrated at Figure 5.13. It can be seen that when oxygen partial pressure is  $2 \times 10^{-2}$  mbar, absorbance increase. As it is understood from that, CuO phase is more absorptive than the Cu<sub>2</sub>O phase. Even though it has good absorptive skills, CuO is not favorable phase for photovoltaics; it is still not clear why Cu<sub>2</sub>O is ideal phase for photovoltaics. But it is known that Cu<sub>2</sub>O's lifetime is longer than CuO's so for overall photovoltaic layer deposition,  $2 \times 10^{-4}$  mbar oxygen pressure will be used to get Cu<sub>2</sub>O phase.

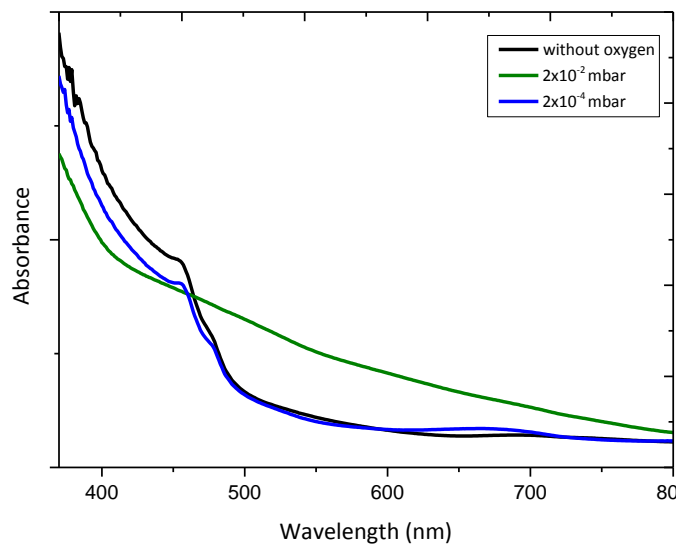


Figure 5.13 Absorbance spectra of copper oxide films prepared at 400°C and different oxygen partial pressures

The copper oxide layer which was deposited under  $2 \times 10^{-4}$  mbar showed absorption edge around 500 nm and its band gap value was estimated to be 2.58 eV by Tauc plot which is given Figure 5.14. As it is seen at Figure 5.13, the film which was deposited under without oxygen partial pressure conditions shows almost same absorbance spectra with the film in  $2 \times 10^{-4}$  mbar. Therefore its band gap is also 2.58 eV as in Figure 5.15. The film which was deposited under  $2 \times 10^{-2}$  mbar oxygen partial pressure shows absorption edge around 700 nm as a difference from other two samples and its band gap was estimated to be 2.07 eV. Invoking that mostly known Cu<sub>2</sub>O band gap is



between 2.0-2.6 eV and CuO band gap between 1.3-2.1 eV the present results also agree with this range.

Film structure and band gap relations were summarized at Table 5.3. Cu<sub>2</sub>O phase's band gap larger than CuO phase's, similar with the literature [52].

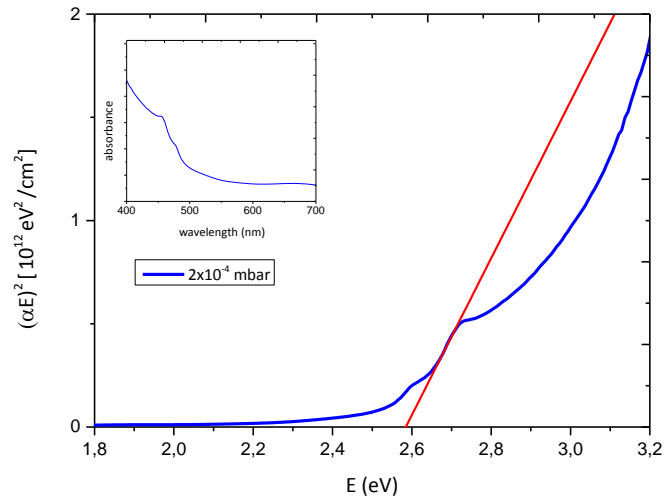


Figure 5.14 Optical direct band gap data of copper oxide, deposited under  $2 \times 10^{-4}$  mbar oxygen partial pressure and its absorbance spectra on the inset graph

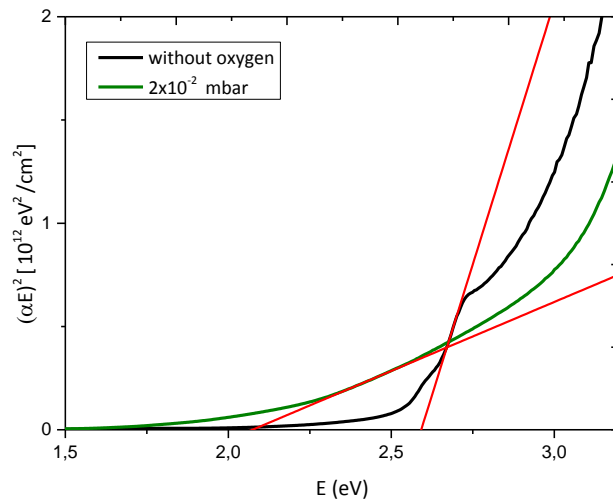


Figure 5.15 Optical direct band gap data of copper oxide, deposited under without oxygen and  $2 \times 10^{-2}$  mbar oxygen partial pressure conditions

Table 5.3 Structure and band gap of copper oxide films

<i>Sample name</i>	<i>Sample Structure</i>	<i>Band gap (eV)</i>
Without oxygen	Cu <sub>2</sub> O-Cu	2.58
2x10 <sup>-4</sup> mbar	Cu <sub>2</sub> O	2.58
2x10 <sup>-2</sup> mbar	CuO	2.07

#### 5.1.4 Overall photovoltaic cell deposition

- **Film structure and morphology**

After optimum deposition parameters defining for both TiO<sub>2</sub> and Cu<sub>2</sub>O layers, overall photovoltaic cell (PV) deposition was carried on ITO substrates and under mentioned conditions on 4.1.6.

As it is seen at Figure 5.16, XRD pattern of PV shows that PV has anatase+rutile phase at n-side and Cu<sub>2</sub>O phase at p-side of the junction. Other peaks; In<sub>2</sub>O<sub>3</sub>, SnO<sub>2</sub> are related with the ITO substrate and for the reason of XRD measurements were taken after gold back contact deposition, Au peak is also seen at the pattern.

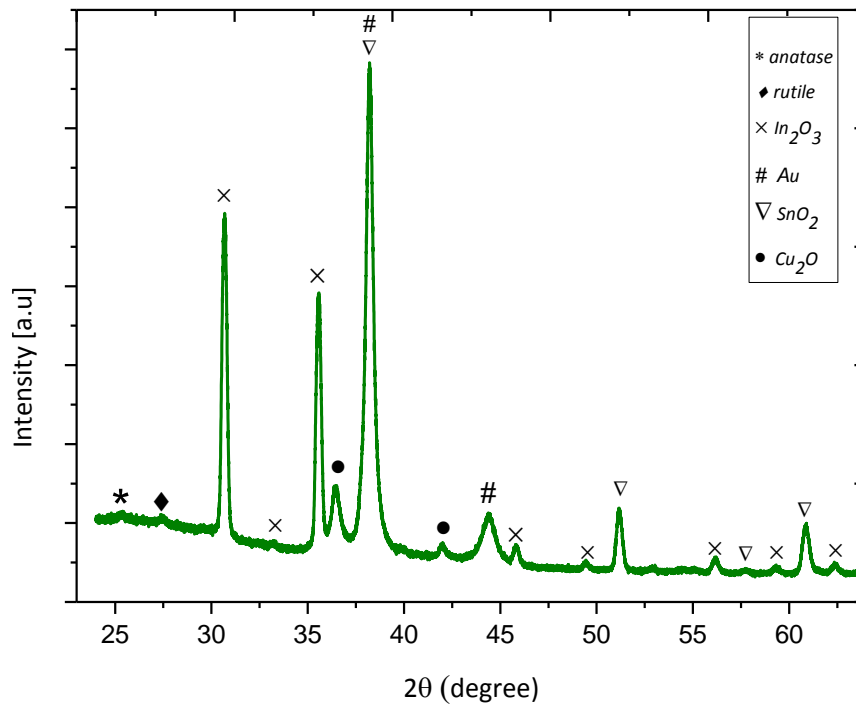


Figure 5.16 XRD pattern of photovoltaic cell

The SEM cross-section image in Figure 5.17 shows that all ITO, TiO<sub>2</sub>, Cu<sub>2</sub>O and gold layers from bottom to up side. TiO<sub>2</sub> and Cu<sub>2</sub>O layers thicknesses are approximately 230 nm and 137 nm.

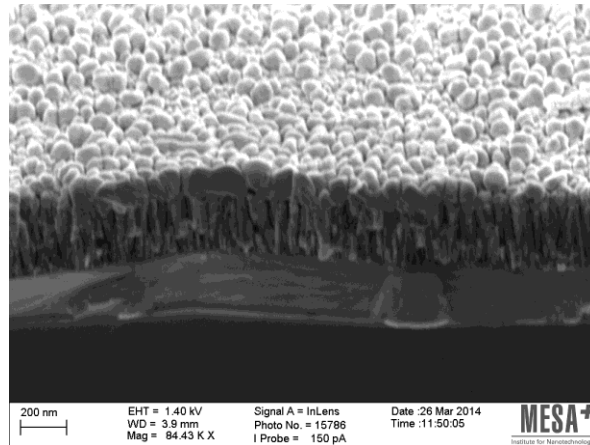


Figure 5.17 SEM image of photovoltaic cell

- **Optical properties**

Figure 5.18 shows that absorption coefficient of the PV with sun AM 1.5 spectrum to understand that the present PV's light absorption behavior in different sunlight regions; as particular ultraviolet (UV), visible and infrared lights. Absorption coefficients of the copper oxide layer were calculated by using equation (2.2). Considering that TiO<sub>2</sub> sample is still transparent after deposition, as seen at the Figure 5.9, during the absorption coefficient calculations and also in Tauc plot only Cu<sub>2</sub>O layer thickness was used.

As related with the band gap of the copper oxide layer, the absorption mostly acts on the early visible and UV regions. Tauc plot is shown at Figure 5.19 with inserted absorbance graph to remind that absorption edge of PV shows up around 500 nm. Band gap of the copper oxide layer on the PV was found to be about 2.43 eV.

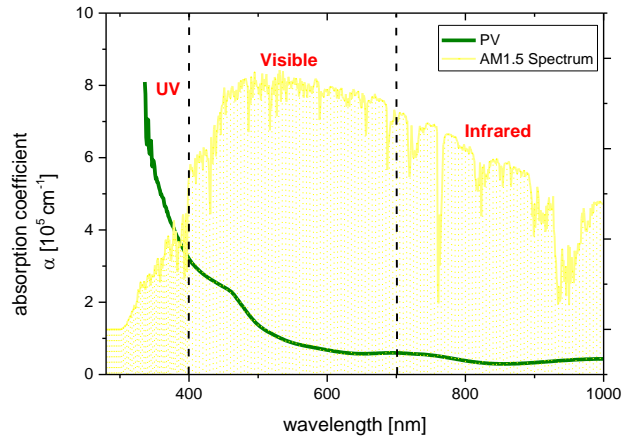


Figure 5.18 Absorption coefficient of copper oxide layer on PV, as comparison with sunlight

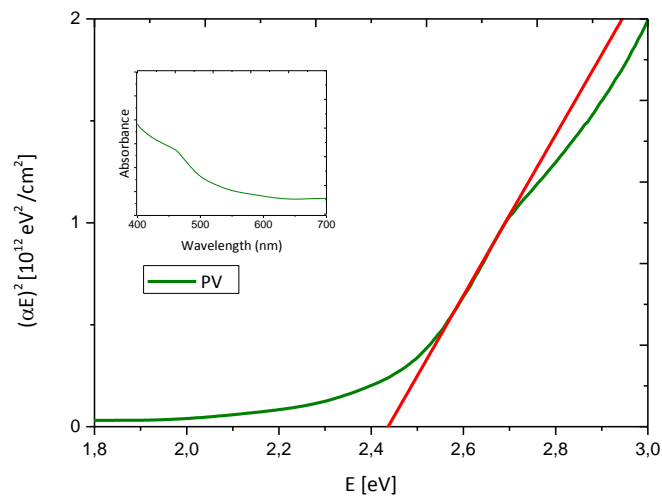


Figure 5.19 Optical direct band gap data of copper oxide layer on PV, and its absorbance spectra on the inset graph

Under same deposition conditions three PV cells were produced. The current-voltage characteristic of cells was measured by using homemade illumination set-up as it is described as heading 4.2. The PVs were illuminated through the glass side and illuminated areas were  $12.5 \text{ mm}^2$ .

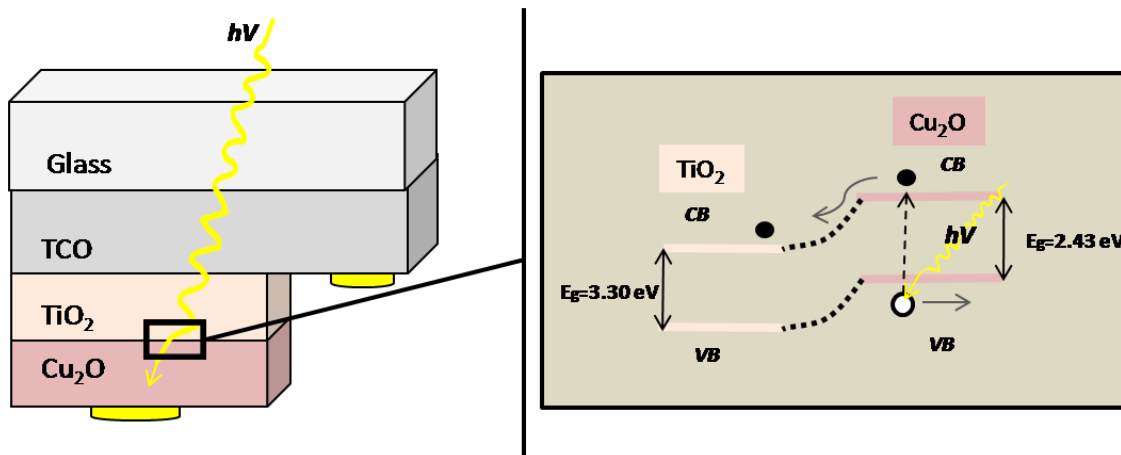


Figure 5.20 Illustration for possible pathway of excited electron in the  $\text{TiO}_2/\text{Cu}_2\text{O}$  heterojunction

During the current-voltage measurements, cells didn't show photovoltaic characteristic. This undesired result might be because of some structural reasons and some technical reasons.

For the structural reasons; copper oxide layer's absorbance edge starts around 500 nm with its 2.43 eV band gap which is nearly the UV region. As it is mentioned above this band gap is in mostly known band gap range for  $\text{Cu}_2\text{O}$  but in the efficient solar cells its band gap nearly 2.0 eV. The band gap of  $\text{TiO}_2$  was estimated approximately 3.30 eV. Under good junction between  $\text{TiO}_2$  and  $\text{Cu}_2\text{O}$ , excited electrons pathway would be in Figure 5.20. But electron flow couldn't occur in present junction. This might be because of the  $\text{TiO}_2$  and  $\text{Cu}_2\text{O}$  band alignment couldn't be achieved at the interface or fast recombination was occurred.

For the technical reasons; it might be probing system was not suitable for the small area PVs. Before the measurements, probe alignment for the contacts might have damaged the PVs' surface and layers were destroyed. However, it might be homemade illumination set-up was not as sensible as to collect weak electrical results of the low efficient PVs and photo conductance tool's light intensity was not enough to simulate the sunlight.

### CONCLUSIONS

In this study,  $\text{TiO}_2/\text{Cu}_2\text{O}$  heterojunction photovoltaic cell was studied. After every deposition, structural and optical inspections were done. Individual layers were discussed detailed in Chapter 5. Therefore in present chapter overall results will be summarized.

$\text{TiO}_2$  layer deposition was done on FTO substrates with  $\text{TiO}_2$  powder and single crystal target under variable pressures and temperatures. In both case, as-deposited films were amorphous. After thermal treatment the anatase phase was achieved. It was seen that increasing the deposition temperature or annealing temperature cause the transparency decrease. Because of the anatase-rutile phase transition by increasing annealing temperature, band gap values were decreased.

To achieve a rich anatase crystalline phase, ITO substrates were also tested. Under variable pressures and temperatures, anatase phase and anatase+rutile mixed phase films were obtained. Although band gap value of anatase phase is higher than anatase's ideal band gap, achieving crystalline phase on as-deposited films makes ITO favorable for  $\text{TiO}_2$  deposition. It might be understood from that crystal structure of ITO is more convenient than the FTO's for  $\text{TiO}_2$  crystal growth.

During  $\text{Cu}_2\text{O}$  deposition, oxygen partial pressure was important parameter for film growth.  $\text{CuO}$  or  $\text{Cu}_2\text{O}$  phases can be obtained by adjusting oxygen pressure. Therefore it was observed that under low oxygen partial pressure  $\text{Cu}_2\text{O}$  occurs. When oxygen partial pressure increased,  $\text{CuO}$  phase appeared. The optical measurements indicated that the absorbance spectra of the  $\text{CuO}$  were higher than that of the  $\text{Cu}_2\text{O}$ 's.

In addition, CuO's band gap was narrower than Cu<sub>2</sub>O phase's as it is similar with many reports.

Overall photovoltaic cell deposition was done on ITO substrates. Deposition parameters which were defined during the deposition of individual layers were applied for overall photovoltaic cell. Anatase and Cu<sub>2</sub>O crystals were achieved. Copper oxide absorption coefficient and band gap were calculated after optical measurements of PV. It was assumed that TiO<sub>2</sub> band gap was similar with the sample which was deposited under same conditions. Both Cu<sub>2</sub>O and TiO<sub>2</sub> layers' band gap values higher than their mostly known band gaps. It might be because of the poor crystallinity of films.

Electrical behavior of PV was measured by using a homemade illumination set-up. No photovoltaic response was observed. Structural reasons for this unexpected result might be poor absorptive copper oxide layer, ineffective TiO<sub>2</sub>/Cu<sub>2</sub>O junction and fast recombination. On the other way, because of the some technical reasons, electrical signals from PV might not be detected. These reasons might be low irradiance of the illumination set-up and difficulties during the probing.

To overcome the structural reasons thicker copper oxide layer deposition could be processed and for sensitive measurements of the thin films illumination set-up improvements are essential. These improvements should involve light changing and more sensitive electrical signal collector for nanoscale results.

## REFERENCES

---

- [1] International Energy Agency (IEA), (2011). Solar Energy Perspectives, 612011251P1, Paris.
- [2] William, S. ve Hans, J.Q., (1961). "Detailed Balance Limit of Efficiency of p-n Junction Solar Cells", *Journal of Applied Physics*, 32:510-519.
- [3] European Photovoltaic Industry Association (EPIA), (2013). Global Market Outlook For Photovoltaics, Brussels.
- [4] Rothwarf, A. ve Böer, K.W., (1975). "Direct Conversion of Solar Energy Through Photovoltaic Cells", *Progress in Solid State Chemistry*, 10, Part 2: 71-102.
- [5] Rappaport, P., (1959). "The Photovoltaic Effect And Its Utilization", *Solar Energy*, 3: 8-18.
- [6] Hecht, J. (2008) Introduction and Overview, in *Understanding Lasers: An Entry-Level Guide*, Third Edition, John Wiley & Sons, Inc., Hoboken, NJ, USA. doi: 10.1002/9780470332306.ch1
- [7] Dong-Kyun, S. ve Roald, H., (1999). "Direct and indirect band gap types in one-dimensional conjugated or stacked organic materials", *Theoretical Chemistry Accounts: Theory, Computation, and Modeling (Theoretica Chimica Acta)*, 102:23-32.
- [8] Gray, J. L. (2011) The Physics of the Solar Cell, in *Handbook of Photovoltaic Science and Engineering*, Second Edition (eds A. Luque and S. Hegedus), John Wiley & Sons, Ltd, Chichester, UK. doi: 10.1002/9780470974704.ch3
- [9] Tauc, J. Grigorovici, R. and Vancu, A., (1966). "Optical Properties and Electronic Structure of Amorphous Germanium", *Physica Status Solidi (b)*, 15: 627-637.
- [10] Diana, M. Tasca, M. Delibas, M. and Rusu, G.I., (2000). "On The Structural Properties And Optical Transmittance Of TiO<sub>2</sub> R.F. Sputtered Thin Films", *Applied Surface Science*, 156:200-206.
- [11] Electronics Tutorials, Available at: [http://www.electronics-tutorials.ws/diode/diode\\_1.html](http://www.electronics-tutorials.ws/diode/diode_1.html). Accessed 25 March, 2014.
- [12] Honsberg, C. and Bowden S., Photovoltaic Education Network, Available at: <http://www.pveducation.org>. Accessed 14 January, 2014.



- [13] Hoffmann, M. Martin, S. Choi, W. and Bahnemann D., (1995). "Environmental Applications Of Semiconductor Photocatalysis", Chemical Reviews, 95:68-96.
- [14] "Solar Cell Operational Principles", Available at: <https://wiki.engr.illinois.edu/download/attachments/220434772/CH4SolarCellOperationalPrinciples.pdf?version=1&modificationDate=1365447090898>. Accessed 20 March, 2014.
- [15] Gueymard, C.A. Myers, D. ve Emery, K., (2002). "Proposed Reference Irradiance Spectra For Solar Energy Systems Testing", Solar Energy, 73:443-467.
- [16] Green, M.A., (1987). "High Efficiency Silicon Solar Cells", Springer: 681-687.
- [17] Wikipedia, Solar Cell, Available at: [http://en.wikipedia.org/wiki/Solar\\_cell](http://en.wikipedia.org/wiki/Solar_cell). Accessed 30 January 2014
- [18] ENF Solar, (2013), Available at: <http://www.enfsolar.com/news/Small-Chinese-Solar-Manufacturers-Decimated-in-2012>. Accessed 31 January, 2014.
- [19] Energy.GOV, U.S Department of Energy, Available at: <http://energy.gov/eere/sunshot/sunshot-initiative>. Accessed 4 February 2014.
- [20] Solar Town Learning, Available at: <http://www.solartown.com/learning/solar-panels/advantages-make-thin-film-solar-panels-shine>. Accessed 3 February, 2014.
- [21] Dubey, S. Sarvaiya, J. and Seshadri, B., (2013). "Temperature Dependent Photovoltaic (PV) Efficiency and Its Effect on PV Production in the World—A Review", Energy Procedia, 33:311-321.
- [22] Jafari Fesharaki, V., Dehghani, M., Jafari Fesharaki, J., (2011). "The Effect of Temperature on Photovoltaic Cell Efficiency", Proceedings of the 1st International Conference on Emerging Trends in Energy Conservation – ETEC, Tehran, Iran, 20-21 November 2011.
- [23] Ample Sun, Ample Sun Technology, Available at: <http://www.ample-sun.com/html/item/15.html>. Accessed 3 February 2014.
- [24] GIGAOM, GIGAOM Research, Available at: <http://gigaom.com/2013/02/26/first-solars-new-world-record-for-solar-cell-efficiency-and-why-its-important/>. Accessed 3 February, 2014.
- [25] Science Daily, Thin film solar cells: New world record for solar cell efficiency, Available at: <http://www.sciencedaily.com/releases/2013/01/130118064733.htm>. Accessed 07 April, 2014.
- [26] Fraunhofer, World Record Solar Cell with 44.7% Efficiency, Available at: [http://www.ise.fraunhofer.de/en/press-and-media/press-releases/presseinformationen-2013/world-record-solar-cell-with-44.7-efficiency?set\\_language=en](http://www.ise.fraunhofer.de/en/press-and-media/press-releases/presseinformationen-2013/world-record-solar-cell-with-44.7-efficiency?set_language=en). Accessed 21 March, 2014.
- [27] O'Regan, B. and Grätzel, M., (1991). "A Low-Cost, High-Efficiency Solar Cell Based On Dye-Sensitized Colloidal TiO<sub>2</sub> Films", Nature, 353: 737-740.

- [28] Abd Elgani, R. Hilo, M.H.M. Al Hassan, A. and Abd Allah M.D., (2012). "Effect Of Doping Concentration On The Performance of Solar Cell Constructed From (Muscovite/TiO<sub>2</sub>/Dye/Al)", 5:52-56.
- [29] Osborne, M., (2010)., PVTECH News, Available at: [http://www.pv-tech.org/news/nrel\\_validates\\_konarkas\\_8.3\\_power\\_plastic\\_efficiency\\_record](http://www.pv-tech.org/news/nrel_validates_konarkas_8.3_power_plastic_efficiency_record). Accessed 25 February, 2014.
- [30] Rühle, S., Andersan A., Barad H., Kupfer B., Bouhadana, Y., Hodesh E. and Zaban, A., (2012). "All-Oxide Photovoltaics", The Journal of Physical Chemistry Letters, 3:3755-3764.
- [31] Olsen, L. Addis, F. ve Miller, W., (1982). "Experimental And Theoretical Studies of Cu<sub>2</sub>O Solar Cells", Solar cells, 7:247-279.
- [32] Tadatsugu, M. Yuki, N. Toshihiro, M. ve Jun-ichi, N., (2011). "High-Efficiency Oxide Solar Cells with ZnO/Cu<sub>2</sub>O Heterojunction Fabricated on Thermally Oxidized Cu<sub>2</sub>O Sheets", Applied Physics Express, 4:062301.
- [33] Dongdong, L. Chung-Jen, C. Suvil, D. Pai-Chun, C. Etienne, M. ve Jia, G.L., (2011). "Prototype of a Scalable Core–Shell Cu<sub>2</sub>O/TiO<sub>2</sub> Solar Cell", Chemical Physics Letters, 501:446-450.
- [34] Musselman, K. Wisnet, A. Iza, D. Hesse, H. Scheu, C. MacManus-Driscoll, J. and Schmidt-Mende, L., (2010). "Strong Efficiency Improvements In Ultra-Low-Cost Inorganic Nanowire Solar Cells", Advanced Materials (Deerfield Beach, Fla.), 22: E254-E258.
- [35] Sajad, H. Chuanbao, C. Zahid, U. Zhuo, C. Ghulam, N. Waheed, S.K. Zulfiqar, A. Faheem, K.B. and Tariq, M., (2012). "Fabrication And Photovoltaic Characteristics of Cu<sub>2</sub>O/TiO<sub>2</sub> Thin Film Heterojunction Solar Cell", Thin Solid Films, 522:430-434.
- [36] Cheng-Chiang, C. Lung-Chien, C. and Yi-Hsuan, L., (2012). "Fabrication and Optoelectrical Properties of IZO/Cu<sub>2</sub>O Heterostructure Solar Cells by Thermal Oxidation", Advances in Condensed Matter Physics, 2012, ID:129139.
- [37] Hiroki, K. Takeo, O. Tsuyoshi, A. Atsushi, S. Balachandran, J. and Jhon, C., (2011). "Fabrication and Characterization of CuO-based Solar Cells", Journal of Materials Science Research, 1:138-143.
- [38] Seung Ki, B. Ki Ryong, L. and Hyung Koun, C., (2013). "Oxide p-n Heterojunction of Cu<sub>2</sub>O/ZnO Nanowires and Their Photovoltaic Performance", Journal of Nanomaterials, 2013, ID:421371.
- [39] Rühle, S. Barad, H. Bouhadana, Y. Keller, D. Ginsburg, A. Shimanovich, K. Majhi, K. Lovrincic, R. Anderson, A. and Zaban, A., (2014). "Combinatorial Solar Cell Libraries For The Investigation of Different Metal Back Contacts For TiO<sub>2</sub>-Cu<sub>2</sub>O Hetero-Junction Solar Cells", Physical Chemistry Chemical Physics : PCCP, 16:7066-7073.
- [40] Robert, W.S. Theodor, S. and Rainer, W., (2004). "Chemical Solution Deposition of Electronic Oxide Films", Comptes Rendus Chimie, 7:433-461.

- [41] Niranjan, S. Parija, B. and Panigrahi, S., (2009). "Fundamental Understanding and Modeling of Spin Coating Process: A Review", Indian Journal of Physics, 83:493-502.
- [42] Hee Park, J. (2001). Chemical Vapor Deposition, First Edition, ASM International, Canada.
- [43] Laboratory for Advanced Molecular Processing, Chemical Vapor Deposition/Atomic Layer Deposition, Available at: <http://phome.postech.ac.kr/user/indexSub.action?codyMenuSeq=69392&siteId=lamp&menuUIType=sub>. Accessed 06 March, 2014.
- [44] Simon, A.H., (2011)., Handbook of Thin Film Deposition Techniques, Processes and Technologies, Third Edition, Waltham [Mass.] : William Andrew, Oxford.
- [45] Direct Vacuum, Magnetron Sputtering Technology, Available at: <http://www.directvacuum.com/sputter.asp>. Accessed 14 March, 2014.
- [46] Eason, R., (2007). Pulsed Laser Deposition Of Thin Films: Applications-Led Growth Of Functional Materials, John Wiley & Sons, New Jersey.
- [47] Krebs, H. Weisheit, M. Faupel, J. and Süske, E., (2003). "Pulsed Laser Deposition (PLD)--A Versatile Thin Film Technique", Advances in Solid State, DOI: 10.1007/978-3-540-44838-9\_36
- [48] Blank, D. Dekkers, M. and Rijnders, G., (2014). "Pulsed Laser Deposition in Twente: From Research Tool Towards Industrial Deposition", Journal of Physics D: Applied Physics, 47:034006.
- [49] Syarif, D. Miyashita, A. Yamaki, T. Sumita, T., Choi, Y. and Itoh H, (2002). "Preparation of Anatase and Rutile Thin Films by Controlling Oxygen Partial Pressure", Applied Surface Science 193:287-292.
- [50] Yong, C. Jian, S. Zhigao, H. Wenlei, Y. Ni, X. Ning, X. Zhifeng, Y. ve Jiada, W., (2013). "Synthesis, Phase Transition and Optical Properties of Nanocrystalline Titanium Dioxide Films Deposited by Plasma Assisted Reactive Pulsed Laser Deposition", Surface and Coatings Technology, 231:180-184.
- [51] Balakrishnan, G. Vengala Rao, B. Rajeswari, S.M. Balamurugan, N. Babu, R.V. ve Song, J.I., (2013). "Effect of Oxygen Partial Pressure on Microstructural and Optical Properties of Titanium Oxide Thin Films Prepared By Pulsed Laser Deposition", Materials Research Bulletin, 48:4901-4906.
- [52] Aiping, C. Hua, L. Xiangcheng, L. Yuhua, L. Guang, Y. ve Peixiang, L., (2009). "Controlled Growth and Characteristics of Single-Phase Cu<sub>2</sub>O And CuO Films By Pulsed Laser Deposition", Vacuum, 83:97-930.
- [53] OHBA's Laboratory, Crystal Structure, Available at: [http://www.geocities.jp/ohba\\_lab\\_ob\\_page/structure6.html](http://www.geocities.jp/ohba_lab_ob_page/structure6.html). Accessed 19 June, 2014.
- [54] Markus, H. Bianca, E. ve Christian, H., (2013). "Band Structure And Phase Stability of The Copper Oxides Cu<sub>2</sub>O, CuO, and Cu<sub>4</sub>O<sub>3</sub>, Physical Review B, 87:115111

- [55] Thien Viet, P. Manohar, R. Andreasson, P. Yuan, P. Junling, W. ve Jinesh, K.B., (2013). "Photocarrier Generation In  $\text{Cu}_x\text{O}$  Thin Films Deposited By Radio Frequency Sputtering", *Applied Physics Letters*, 102:032101.
- [56] Kirchartz, T. ve Rau, U., (2011). *Introduction to Thin-Film Photovoltaics, Advanced Characterization Techniques for Thin Film Solar Cells*. Wiley-VCH Verlag GmbH & Co. KGaA, 1-32.
- [57] Krit, W.-i. ve Pisutti, D., (2012). "Soda-Based Glass Fabricated From Thailand Quartz Sands Doped with Silver Compound", *Optical Materials*, 34:2108-2111.
- [58] Amor, S.B. Baud, G. Besse, J.P. ve Jacquet, M., (1997). "Structural and Optical Properties of Sputtered Titania Films", *Materials Science and Engineering: B*, 47:110-118.
- [59] Kääriäinen, M.L. Kääriäinen, T.O. and Cameron, D.C., (2009). "Titanium Dioxide Thin Films, Their Structure and Its Effect on Their Photoactivity and Photocatalytic Properties", *Thin Solid Films*, 517:6666-6670.
- [60] Li-Jian, M. and Santos, M.P., (1993). "Investigations Of Titanium Oxide Films Deposited by D.C. Reactive Magnetron Sputtering In Different Sputtering Pressures", *Thin Solid Films*, 226:22-29.

## CURRICULUM VITAE

---

### PERSONAL INFORMATION

**Name Surname** : TÜLİN YILMAZ  
**Date of birth and place** : 29/02/1988 İSTANBUL  
**Foreign Languages** : English  
**E-mail** : [tulinylmaz@gmail.com](mailto:tulinylmaz@gmail.com)

### EDUCATION

<b>Degree</b>	<b>Department</b>	<b>University</b>	<b>Date of Graduation</b>
Master	Chemical Engineering,	Yıldız Technical University,	2014
Erasmus	Inorganic Material Science	University of Twente,	2014
Undergraduate	Chemical Engineering,	Yıldız Technical University,	2011
	Environmental Engineering	Yıldız Technical University,	2010
High School	Cibali High School		2006

### WORK EXPERIENCE

<b>Year</b>	<b>Corporation/Institute</b>
2011-2013	İNERÇEVRE & İNERGALVANO Industry Trade Limited Company

## **PUBLISHERMENTS**

### **Papers**

1. Yetilmezsoy, K., Turkdogan, F.I., Gunay, A., Yilmaz, T., Kaleli, M., Medicinal plants grown in soil amended with struvite recovered from anaerobically pretreated poultry manure wastewater, The Journal of Animal & Plant Sciences , Vol. 23, Issue 1, pp. 261-270, (2013)

### **AWARDS**

1. Yıldız Technical University, Faculty of Civil Engineering, Environmental Engineering Department, Top Student of Department, 2009-2010